

UNCLASSIFIED



Australian Government
Department of Defence
Defence Science and
Technology Organisation

Modification of the Gurney Equation for Explosive Bonding by Slanted Elevation Angle

C. Choi¹, M. Callaghan², P. van der Schaaf¹, H. Li³ and B. Dixon¹

¹ Land Division
Defence Science and Technology Organisation

² School of Mechanical, Aerospace and Civil Engineering
The University of Manchester

³ Faculty of Engineering
University of Wollongong

Defence Science and Technology Organisation

DSTO-TR-2960

ABSTRACT

Using a modified Gurney equation, explosive bonding has been achieved with an angle of elevation between two plates and utilising an explosive charge with supersonic detonation velocity. Two joint combinations were produced with superaustenitic steel as the flyer plate and either Transformation Induced Plasticity (TRIP) steel or armour steel, designated 'HARD steel' in this work, as alternatives for use as bottom plates. Good metallurgical bonds were created for each joint combination, with the formation of wave-type microstructural morphology at the joint interface. As a result of localised severe plastic deformation and subsequent work-hardening within the steels the microstructures at the joint interface revealed complex metallurgical features, which correlated strongly with hardness variation.

RELEASE LIMITATION

Approved for Public Release

UNCLASSIFIED

UNCLASSIFIED

Published by

Land Division

DSTO Defence Science and Technology Organisation

506 Lorimer St

Fishermans Bend, Victoria 3207 Australia

Telephone: 1300 333 362

Fax: (03) 9626 7999

© Commonwealth of Australia 2014

AR-015-932

April 2014

APPROVED FOR PUBLIC RELEASE

UNCLASSIFIED

Modification of the Gurney Equation for Explosive Bonding by Slanted Elevation Angle

Executive Summary

The Gurney equation has been used to optimise the explosive bonding parameters necessary to achieve successful explosive bonding of metals for many years. However, the equation is only applicable when the two plates to be bonded are parallel and the detonation velocity of the explosive charge used is within a narrow range.

This paper proposes a modification of the Gurney equation for the explosive welding of metallic materials to allow for circumstances where the plates to be bonded are not parallel and charge detonation rates are higher than those allowed for by the equation.

With the application of the modified Gurney equation, the explosive welding of two plate material combinations was achieved. Both plate combinations used a superaustenitic plate as the flyer plate and either a Transformation Induced Plasticity (TRIP) steel or an armour steel designated 'HARD steel', as the bottom plate. Good metallurgical bonds were created for both material combinations, and the formation of a wave-type joint morphology (a characteristic of the explosive welding process) occurred at the joint interface. The joint microstructures revealed complex metallurgical features developed as a consequence of the localised severe plastic deformation and work-hardening experienced during the welding process. This was confirmed by hardness testing in the region of the weld.

Explosive welded plates represent a potential improvement in armour plate properties which will be explored in future work.

UNCLASSIFIED

Authors

Chang Ho Choi

Land Division

Defence Science and Technology Organisation

Chang-Ho Choi obtained a Master's degree in Materials Science at Oregon State University and undertook PhD study at the University of Illinois and later at the University of New South Wales, where he received a PhD with a thesis on superconductors. He has been employed as a materials scientist at DSTO Maritime Platforms Division since 1998. During the period 1998 to 2006, he worked with the metallurgy section. From 2006 to 2009, he worked in the biology section and from 2009 onward, in the Armour Mechanics and Vehicle Survivability group at Maritime Division and later Land Division.

Mark Callaghan

School of Mechanical, Aerospace and Civil Engineering

The University of Manchester

Mark Callaghan undertook his PhD at the Australian Nuclear Science and Technology Organisation, researching high temperature fatigue behaviour and modelling of ferritic pressure vessel steel, for which he was awarded the degree at the University of Technology, Sydney in 2009. He joined the University of Wollongong in 2008 as a Research Fellow, where he undertook research into armour and high strength steels subjected to static and dynamic loadings, weldability and welding metallurgy of these materials as a function of welding processes and simulations. In 2012, Mark was appointed as Research Associate at The University of Manchester, researching thick-walled corrosion resistant materials for high-temperature high-pressure service.

UNCLASSIFIED

UNCLASSIFIED

Paul van der Schaaf

Military Loads Group

Maritime Division

Defence Science and Technology Organisation

Paul van der Schaaf was awarded a BSc(Hons) majoring in physics by the University of Western Australia. With the Defence Science and Technology Organisation he works in the areas of underwater explosive shock and bubble dynamics, the dynamic response of structures, and instrumentation & measurement. He has also worked in the areas of impact dynamics, finite element analysis, shock standards, fault tree analysis, naval platform vulnerability and visual encryption.

Huijun Li

Faculty of Engineering

University of Wollongong

Huijun Li obtained his PhD degree in 1996 at University of Wollongong; he then joined the CRC on Materials Welding and Joining as a postdoctoral research fellow at the University of Wollongong. In 2000, he took a research scientist position at the Materials Division, ANSTO (Australian Nuclear Science and Technology Organisation), he worked on a wide range of research projects in conjunction with the CRC on Welded Structures, CRC CAST3, CRC Rail, British Nuclear Research Organisation and American national laboratories. Huijun Li started working at University of Wollongong from July 2008; he is a full time research only staff with Defence Materials Technology Centre and Energy Pipeline CRC.

Brian Dixon

Land Division

Defence Science and Technology Organisation

Brian Dixon is a metallurgist in the Land Division of Defence Science and Technology Organisation. He has been employed at DSTO since 1978, undertaking experimental development and fundamental studies into weld metal solidification cracking in steels and stainless steels. He has also undertaken extensive work on improving the weld zone toughness of high strength steels. During 1989 and 1990 Brian worked at Kockums

UNCLASSIFIED

UNCLASSIFIED

Laboratory in Sweden as part of DSTO's contribution to the submarine project. Since 2001, Brian has worked in a number of developmental positions, including Director, Program Office (Maritime), STCC for M1 and M6 and S&T Adviser for JP 2048. He is currently in Land Division as a research fellow.

UNCLASSIFIED

Contents

1. INTRODUCTION.....	1
2. EXPERIMENTS AND FUNDAMENTALS	2
2.1 Materials and Experimental Methodologies	2
2.2 Properties of Explosive Material.....	5
2.3 Calculation of Flyer Plate Velocities	5
2.3.1 Velocity of the contact point between the inclined flyer plate and the bottom plate	6
2.3.1.1 Dynamic bend angle	6
2.3.1.2 Inclined flyer plate.....	7
2.3.1.3 Contact velocity	7
3. RESULTS AND DISCUSSION	9
3.1 Explosive bonding process.....	9
3.2 Investigation of microstructural and hardness variation of explosive welded joints	14
3.2.1 Microstructural variation	14
3.2.2 Joint Hardness Variation	24
4. CONCLUSIONS.....	28
5. ACKNOWLEDGEMENTS	29
6. REFERENCES	29
Gurney Equation	31
Cylindrical geometry.....	31
Critical impact pressure	32

UNCLASSIFIED

This page is intentionally blank

UNCLASSIFIED

1. Introduction

Explosive welding is a solid-state metal-joining process that uses explosive force to create a metallurgical bond between two metal components. This occurs by cold working because there is insufficient time for the heat transfer from the explosion [1]. Explosive welding is well known for its capability to directly join a wide variety of similar [2-4] and dissimilar [5-7] combinations of metals that cannot be joined as efficiently by other techniques. The lists of metallic materials and material combinations that can be successfully joined include steel, aluminium, titanium, nickel, copper, and metallic glass, among many others. Over 260 various similar and dissimilar metal and alloy combinations have been welded by using explosive welding techniques [8].

The Gurney equations [9] are a set of mathematical formulas used in explosives engineering to relate how fast an explosive will accelerate a surrounding layer of metal or other material when the explosive detonates (refer to Appendix I). This determines how fast fragments are released by military explosives, how quickly shaped charge explosives accelerate their liners inwards, and in other calculations such as explosive welding where explosives force two metal sheets together and weld them. With explosive welding, the Gurney equations have been used for more than 50 years to characterize the dissimilar and similar joint plates, however, the equation is based on empirical data only. Gurney [9] argued that the governing factor for explosive welding was the ratio between the mass of the fragments or clad metal (M) and the mass of the explosive (C) under the simple assumption that the chemical energy of the explosive was transformed into kinetic energy of explosive products and metal fragments. He concluded that the velocity of fragments to the ratio C/M and the shape of explosive charges are the most influential factors to determine the explosive welding [10]. Unfortunately, the standard Gurney formula can only be used when two plates (flyer and bottom) are parallel to each other as shown in Figure 1. Furthermore, the equation does not consider the effects of the bottom plate hardness on bond integrity.

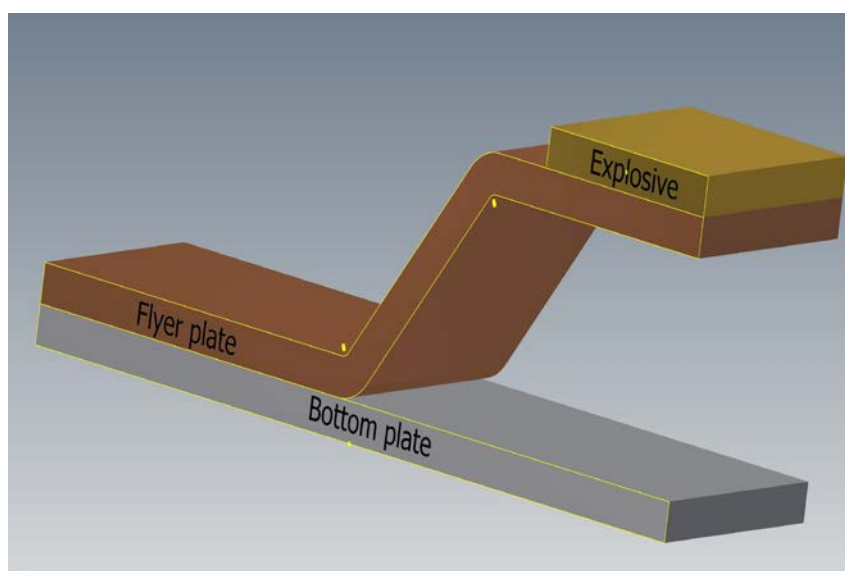


Figure 1: A schematic of the explosive welding process

Explosive welding occurs when two plates collide at high velocity and at oblique angles causing a jetting or spraying action of metal at the apex of the collision [11]. Jetting is associated with plastic flow caused by high pressure at the collision interface. This jet becomes the critical element in explosive welding. Another characteristic of explosive welding is that the jet cleanses the surfaces of all surface contaminants and forces them into direct welding. For this reason, any cleaning preparation of a test coupon is theoretically unnecessary.

It is argued [10] that when the detonation velocity is such that the collision velocity is supersonic with regard to the material, then no jet can occur and Carpenter et al [12] indicated that explosives with detonation velocities greater than 120 % of the sonic velocity of the metal should not be used. If the argument is true, for example, it is not practical to bond two plates with PE4 explosive because the detonation velocity of PE4 charge is about 7.9 km/s, which is much higher than the sonic velocity of normal mild steel (5.9 km/s). However, the Gurney approach [9] only applies to plates set up parallel to each other prior to explosive bonding. This investigation looks at the possibility of using explosive material with a detonation velocity higher than the sound velocity of the bonded materials in combination with plates presented at an angle to each other.

The purpose of this paper is therefore to determine if the formulas developed by Gurney [9] can be modified to be successfully applicable when the two plates to be joined are presented with an angle of elevation to each other.

The joints produced by the explosive bonding process were investigated through microstructural analyses and hardness measurements, to assess the bonding interface, as well as the microstructural and hardness variation for each plate material.

2. Experiments and Fundamentals

2.1 Materials and Experimental Methodologies

Five explosive bonding experiments were undertaken, using flyer plate material, superaustenitic steel and two alternative bottom plate materials, Transformation Induced Plasticity (TRIP) steel or high strength, high hardness HARD steel. All steels possess different chemistry, heat-treatment and mechanical properties. As shown in Tables 1 and 2.

Table 1: Chemical compositions (wt%) of superaustenitic steel, TRIP steel and HARD steel

Material	C	S	P	Si	Mn	Cr	Mo	Ni	N	Nb
Superaustenitic steel ¹	<0.030	<0.005	<0.025	<1.0	4.0/6.0	20/21.5	3.0/3.5	15/17	0.20/0.35	<0.25
TRIP steel ²	<0.185	-	-	0.55	2.30	0.1	0.25	0.08	-	-
HARD steel ²	<0.22	<0.005	<0.015	<0.5	<1.5	<1	<0.6	<2.0	-	-

1: flyer plate and 2: target (bottom) plate

Table 2: Typical mechanical properties of superaustenitic steel, TRIP steel and HARD steels

Material	Yield strength (MPa)	Ultimate tensile strength (MPa)	Elongation (%)
Superaustenitic steel	430	700-950	>35
TRIP steel	640	780	14
HARD steel	1150	1450	13

The first four explosive welding experiments were conducted with a TRIP steel bottom plate and a superaustenitic steel flyer plate. These plates were water jet cut to dimensions of 50 mm × 150 mm × 2.0 mm and 150 mm × 150 mm × 8.5 mm, respectively. The fifth explosive welding experiment incorporated a HARD steel (bottom plate) and a superaustenitic steel (flyer) plate with dimensions of 300 mm × 300 mm × 4.2 mm and 300 mm × 300 mm × 8.5 mm, respectively. The explosive charge was contained in a wooden box with dimension of 150 mm × 150 mm × 100 mm for the superaustenitic steel / HARD steel joint combinations and 300 mm × 300 mm × 100 mm for the final sample. Table 3 shows the details of the plate preparation used for explosive bonding tests.

Table 3: Details of the plate preparation for explosive bonding

No	Joint combination (Top plate – Bottom plate) (mm: nominal thickness)	Plate Angle (degree)	Charge Weight (kg)	Charge Thickness (mm)	Bonded area (mm)
1	S ¹ steel (8.5) – TRIP steel (2.0)	10	0.3	8	150x150
2	S steel (8.5) – TRIP steel (2.0)	10	0.6	16	150x150
3	S steel (8.5) – TRIP steel (2.0)	10	0.9	24	150x150
4	S steel (8.5) – TRIP steel (2.0)	15	0.6	16	150x150
5	S steel (8.5) – HARD steel (2.0)	15	2.4	16	300 x300

1: S defines 'Superaustenitic'.

The flyer plate was placed on the top of the bottom plate for each test with either a 10° or a 15° plate angle (Figure 2). Figure 2 shows the schematic of the material preparation for the explosive bonding experiments.

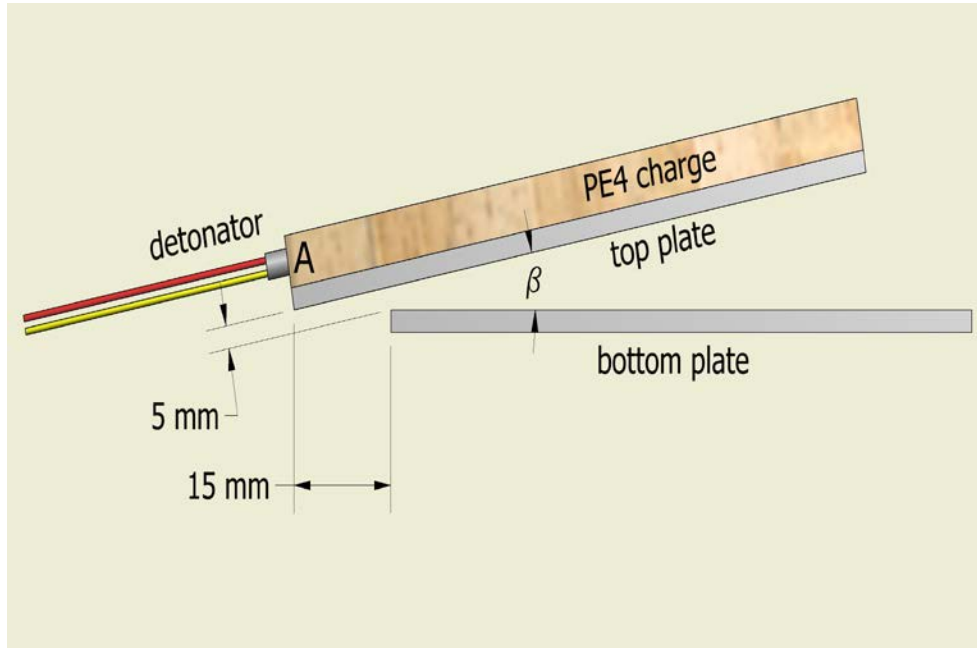


Figure 2: A schematic (not to scale) of the configuration and position of flyer (top) and bottom plates, together with PE4 charge. β represents the plate angle

As shown in Figure 2, the flyer plate was located 15 mm beyond the left hand edge of the bottom plate. This was done to optimise the jetting action developed between the two plates. The region marked 'A' indicates the location of the detonator, which was placed in a drilled hole in the explosive, 10 mm above the top plate. The test apparatus was located on a 20 mm rubber mattress for shock absorbing purposes.

Following explosive bonding, metallographic preparation was undertaken to examine the microstructural evolution through the plate thickness. Firstly, a section was wire-cut from the joined plates in order to investigate the joint cross-section. Grinding was then undertaken using 800 to 1200 grade SiC abrasive papers with water as a lubricant. This was followed by polishing with progressive diamond suspensions of 6 μm , 3 μm , and 1 μm using a water-based lubricant. The excellent corrosion resistance of the superaustenitic steel, which possesses high levels of chromium and nickel, means that this material is noble with respect TRIP and HARD steels. Therefore, the joint microstructures needed to be revealed with a 2-step etching process. Firstly the TRIP steel and HARD steel microstructures were etched using 2% Nital followed by metallographic examination and photographic recording. Secondly, the superaustenitic steel microstructures were revealed using an electrolytic etchant of 10 g oxalic acid dissolved in 100 ml distilled water, at 4V for between 1 to 3 minutes. The TRIP steel/HARD steel etched microstructure was destroyed during this second process. Microstructural analysis of the joints and interfaces were undertaken via optical microscopy, at a variety of magnifications using a Leica DMR light microscope.

The hardness variation of each joint in the through plate thickness direction was also characterised using Vickers microhardness testing, using a 200g load ($\text{HV}_{200\text{g}}$) and a Leco microhardness indenter.

2.2 Properties of Explosive Material

PE4 material has an explosive charge almost equivalent to C-4 explosive. PE4 material is made up of explosives, plastic binder and plasticizer. The detonation velocity of PE4 charge in use is 7,900 m/s.

2.3 Calculation of Flyer Plate Velocities

Flyer plate velocities can be calculated from the Gurney equation [9]. Gurney assumed that the driven metal was accelerated perpendicular to the direction of the detonation propagation and used a specific energy with a characteristic value for each explosive.

Following Meyers [13], the explosive test configuration presented in Figure 3 shows the schematic of normal explosive bonding. In this case, the velocity of the collision front (V_C) is equal to the detonation velocity (V_D). This is true only in the parallel plate configuration. The dynamic bend angle δ (refer to Figure 4) is obtained from the detonation and plate velocities V_D and V_P , respectively, by simple geometric considerations. In Figure 3, V_P bisects the angle between the original plate orientation and the deformed plate. Where point A goes to B along V_P point O goes to B along V_C . Thus the triangle OAB is isosceles, and for triangle OBC, there is given.

$$V_P = 2V_D \sin \frac{1}{2} \delta \quad (1)$$

For small dynamic bend angles, Equation 1 is approximately

$$V_P = V_D \sin \delta \quad (2)$$

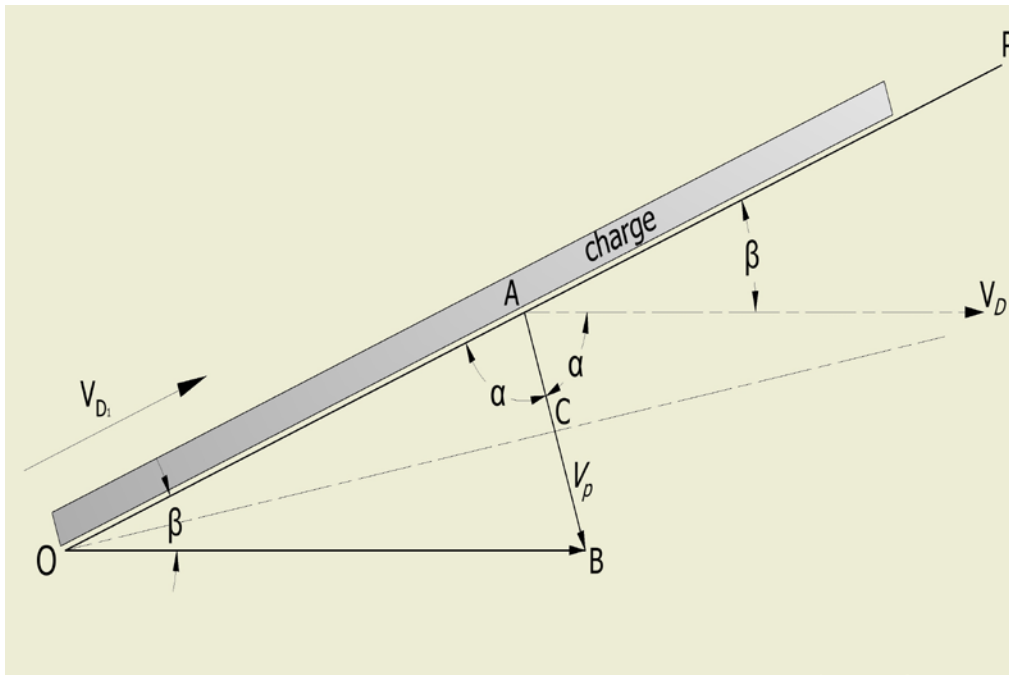


Figure 3: A schematic of the plate setup, vectors and angles between both flyer and bottom plates, in relation to the position of PE4 charge

As shown in Figure 2 and Figure 3, the charge was inclined at an angle β . As previously mentioned, the Gurney equation cannot be used directly, as it is only applicable to parallel plates. However, it is possible to apply this equation with a simple modification to the explosive bonding of non-parallel plates. This is demonstrated in the following sections.

2.3.1 Velocity of the contact point between the inclined flyer plate and the bottom plate

The normal parallel plate explosive welding process requires that the detonation velocity is less than 120% of the sonic velocity of the metal [12]. Should the detonation velocity exceed this limit it is possible to slow the effective speed of the detonation front by inclining the flyer plate to the bottom plate. This allows broader accessibility for selecting explosive materials. In this test, the sonic velocity of the flyer plate and the detonator is 5900 m/s and 7900 m/s, respectively. The ratio between the flyer plate and the detonator is 1.34, which is above the applicable limitation as outlined in [12]. For practical use, the contact velocity may be decreased by controlling the angle β in Figure 3.

2.3.1.1 Dynamic bend angle

The detonation of the backing explosive imparts a velocity to the underlying metal plate which in this case is given by the open-faced sandwich Gurney equation. As the detonation front runs along the back of the plate it creates a hinge in the plate moving at this same velocity with a dynamic bend angle of δ , Figure 4.

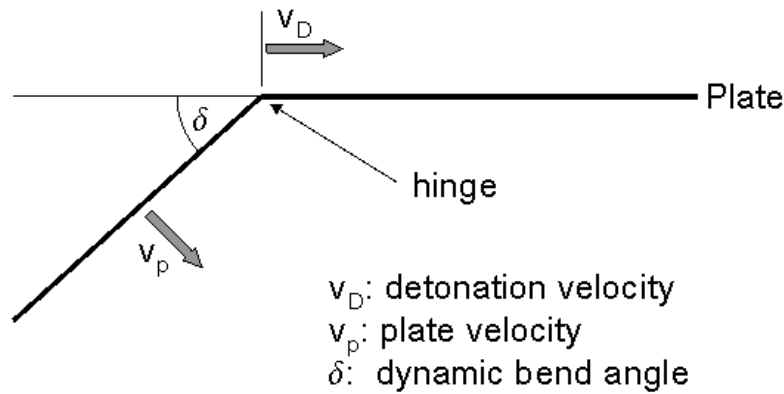


Figure 4: A schematic showing an explosively driven flyer plate with a dynamic bend angle of δ

Rearranging Equation 2 gives the dynamic bend angle δ of the hinge as

$$\delta = \arcsin\left(\frac{v_P}{v_D}\right). \quad (3)$$

2.3.1.2 Inclined flyer plate

The dynamic bend angle δ is dependent on the explosive and flyer plate characteristics. The ratio of the velocity of the contact point of the flyer plate against the base plate to the detonation velocity is determined by δ and the angle of inclination of the flyer plate, β , as shown in Figure 5.

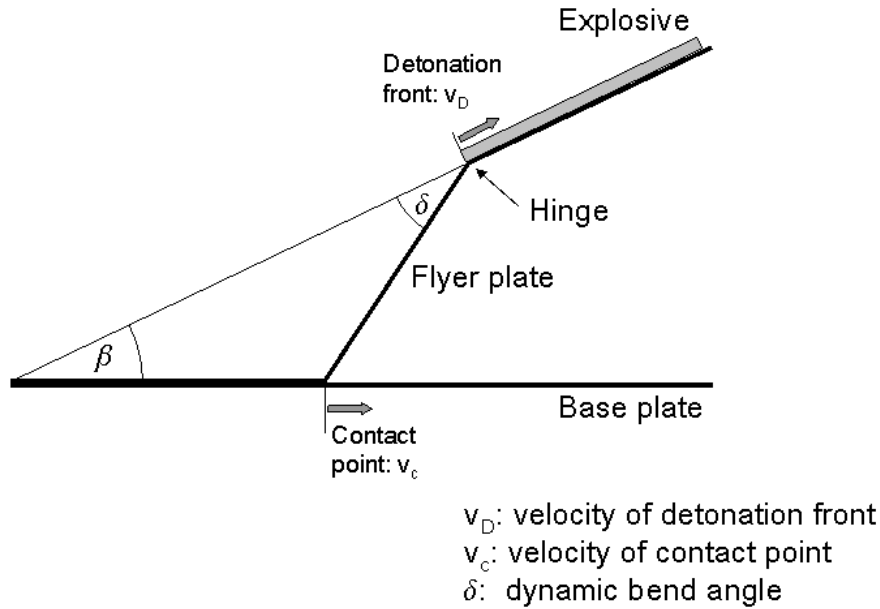


Figure 5: A schematic showing the flyer plate being explosively driven on to the bottom plate with a dynamic bend angle of δ . The velocity of the contact point along the base plate, v_c , is reduced by inclining the flyer plate, here shown at an angle of β .

Following from the geometry shown in Figure 5, the ratio of the velocity of the contact point, which is the *effective* detonation velocity, to the velocity of the explosive's detonation front is

$$\frac{v_c}{v_D} = \cos(\beta) - \sin(\beta) \cdot \cot(\beta + \delta), \quad (4a)$$

which can be simplified to

$$v_c = v_D \cdot \csc(\beta + \delta) \cdot \sin(\delta). \quad (4b)$$

It is required that v_c is less than 120% of the metal's sonic velocity.

2.3.1.3 Contact velocity

Equation 4 shows how the velocity of the contact point, the effective detonation velocity, is slowed by inclining the flyer plate. The ratio of the velocity of the contact point to the detonation velocity of the explosive is plotted for plate inclination angles ranging from 0° to 25° for each of the selected dynamic bend angles of 5° , 10° , 15° , 20° , 25° and 30° (Figure 6) and tabulated in Table 4.

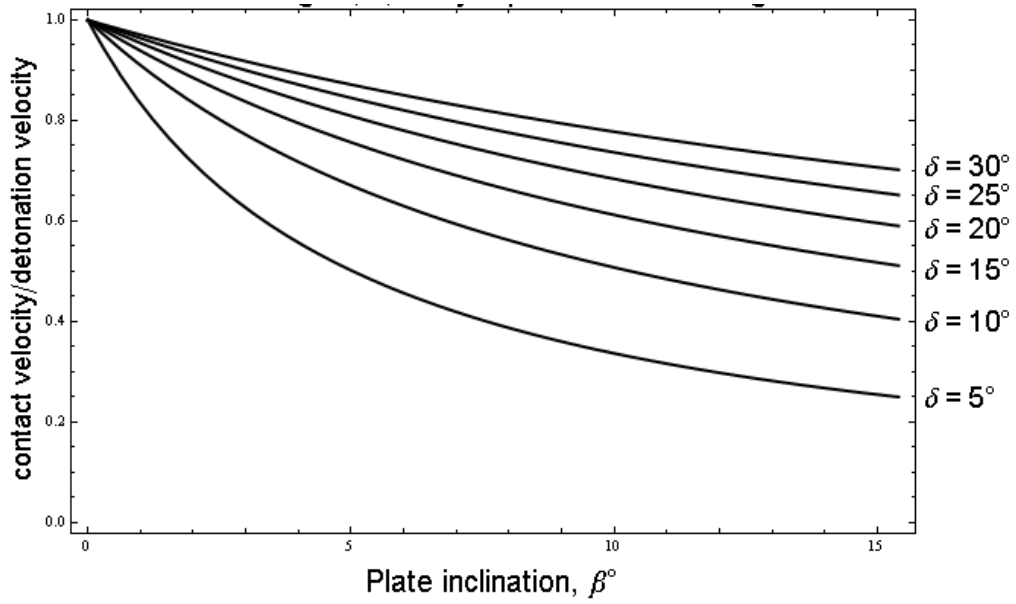


Figure 6: The ratio of the contact velocity to the detonation velocity for selected dynamic bend angles, δ , plotted against flyer plate inclination angle.

Table 4: Contact to detonation velocity ratios for selected dynamic bend angles and plate inclination angles

Plate inclination angle, β°	Dynamic bend angle, δ°					
	5	10	15	20	25	30
0	1	1	1	1	1	1
5	0.5	0.67	0.76	0.81	0.85	0.87
10	0.34	0.51	0.61	0.68	0.74	0.78
15	0.25	0.41	0.52	0.6	0.66	0.71

To calculate the contact velocity, first calculate the ratio of the area density of the flyer plate to the area density of the explosive backing charge,

$$\frac{M}{C} = \frac{\rho_m}{\rho_e} \cdot \frac{t_m}{t_e}, \quad (5)$$

where ρ_m = plate density (kg/m^3), ρ_e = explosive density (kg/m^3), t_m = plate thickness (m) and t_e = explosive thickness (m).

Substitute the expression for the ratio $\frac{M}{C}$, Equation 5, into the equation for the flyer plate velocity V_P , Equation 6,

$$V_P = \sqrt{2E} \left[\frac{1 + (1 + 2M/C)^3}{6(1 + M/C)} + \frac{M}{C} \right]^{-\frac{1}{2}}. \quad (6)$$

Note that V_p has the units of mm/microsecond and follows from the units of the Gurney constant $\sqrt{2E}$. Substitute the flyer plate velocity V_p into Equation 7, the equation for the dynamic bend angle,

$$\delta = \arcsin\left(\frac{V_p}{v_D}\right). \quad (7)$$

Finally, substitute the dynamic bend angle δ with the selected flyer plate inclination angle β into equation 8 for the contact velocity of the flyer plate v_c along the base plate,

$$v_c = v_D \cdot \cos(\beta + \delta) \cdot \sin(\delta). \quad (8)$$

The physical properties of the materials to be used are shown in Table 5, together with the detonation velocity and Gurney constant.

Table 5: Physical properties of the flyer plate material, superaustenitic steel and the explosive, PE4. The detonation velocity and Gurney constant are also shown.

Material	Density(g/cm ³)	Thickness (mm)
Superaustenitic ¹	8.177	8.5
PE4 charge	1.59	16
Detonation velocity D = 7900 m/s Gurney constant = 2.68 mm/μs		

¹flyer plate

3. Results and Discussion

3.1 Explosive bonding process

Five explosive bonding experiments were undertaken to estimate the optimised plate velocity and pressure produced by the PE4 explosive charge. The M/C ratio, plate velocity, estimated pressure, and optimised explosive charge thickness were calculated by using the material properties shown in Table 2 and combining Equation 1 to Equation 7. Table 6 shows the results of the calculated explosive welding parameters. The Gurney equations and the method of the calculated dynamic critical impact pressure are detailed in Appendix A.

Table 6 *The explosive bonding plate parameters*

M/C ¹	Explosive thickness (mm)	V _P ² (m/s)	Contact velocity ³ at $\beta = 10^\circ$ (m/s)	Contact velocity ³ at $\beta = 15^\circ$ (m/s)	Dynamic pressure ⁴ (GPa)	Dynamic pressure shock ⁵ (GPa)
1.6	26.1	1058	3483	2745	4.37	24.35
1.7	24.5	1012	3389	2658	3.99	23.27
1.8	23.2	969	3307	2583	3.66	22.29
1.9	21.9	930	3221	2505	3.37	21.39
2	20.8	893	3143	2435	3.11	20.56
2.1	19.9	860	3076	2376	2.88	19.79
2.2	19	829	3007	2314	2.68	19.07
2.3	18.1	800	2934	2250	2.5	18.41
2.4	17.4	773	2874	2198	2.33	17.79
2.5	16.7	748	2813	2144	2.18	17.21
2.6	16	725	2749	2089	2.05	16.67
2.7	15.4	703	2692	2040	1.92	16.16
2.73	15.3	696	2683	2032	1.89	16.02
2.8	14.9	682	2643	1999	1.81	15.69
2.9	14.4	662	2593	1956	1.71	15.24
3	13.9	644	2541	1912	1.62	14.81
3.1	13.5	626	2499	1876	1.53	14.41
3.2	13	610	2444	1830	1.45	14.03
3.3	12.6	594	2399	1793	1.38	13.67
3.4	12.3	579	2364	1764	1.31	13.33
3.5	11.9	565	2317	1725	1.24	13
3.6	11.6	552	2281	1695	1.19	12.69
3.7	11.3	539	2245	1665	1.13	12.39
3.8	11	526	2207	1634	1.08	12.11
3.9	10.7	515	2169	1603	1.03	11.84
4	10.4	503	2130	1571	0.99	11.59
4.1	10.2	493	2103	1550	0.95	11.34
4.2	9.9	482	2063	1517	0.91	11.1
4.3	9.7	473	2035	1495	0.87	10.88
4.4	9.5	463	2008	1473	0.84	10.66
4.5	9.3	454	1979	1450	0.8	10.45
4.6	9.1	445	1951	1428	0.77	10.25
4.7	8.9	437	1922	1404	0.74	10.05
4.8	8.7	429	1892	1381	0.72	9.87
4.9	8.5	421	1863	1357	0.69	9.69
5	8.3	414	1832	1333	0.67	9.52

1. Ratio of flyer plate mass to charge mass.

2. Flyer plate velocity calculated using open-faced Gurney equation using a Gurney constant of $2.68 \text{ mm} \cdot \mu\text{s}^{-1}$, equation 5. The contact velocities were calculated by Equation 11.

3. Contact velocity of inclined flyer plate calculated using a detonation velocity of $7900 \text{ m} \cdot \text{s}^{-1}$.

4. Dynamic pressure calculated with the Bernoulli equation.

5. Shock pressure.

The overall test results are shown in Table 7, with experimental setup parameters and comments on each test.

Table 7: Test results of the explosive bonding tests

No	Joint combination	Plate Angle (°)	Charge Mass (kg)	Charge Thickness (mm)	Flyer and Target Plate Dimension (mm)	Remarks
1	superaustenitic steel – TRIP steel	10	0.3	8	150x150x2	No bonding
2	superaustenitic steel – TRIP steel	10	0.6	16	150x150x2	good bonding
3	superaustenitic steel – TRIP steel	10	0.9	24	150x150x2	No bonding
4	superaustenitic steel – TRIP steel	15	0.6	16	150x150x2	Very good bonding
5	superaustenitic steel – HARD steel	15	2.4	16	300x300x4.7	good bonding

Equation A7 and Equation A10 in Appendix A were used as an upper and lower bound threshold windows to measure an optimised thickness of explosive charge layer, flyer velocity. From Equation 6, $M/C = (8.177/1.59) * (8.5/16) = 2.73$. Inserting this value into Equation 7, one can calculate the plate velocity which is close to 696.15 m/s. PE4 detonation velocity is approximately 7900 m/s.

Four explosive charges were selected (300 g, 600 g, 900 g for superaustenitic steel - TRIP steel combination, and 2.4 kg for superaustenitic steel - HARD steel). The 300g charge weight was selected to determine whether or not jetting would be created at this pressure range. The explosion with 300 g charge weight (dimension of the flyer plate: 150 mm x 150 mm plates) with 8 mm explosive charge thickness showed no bonding at all. The 900 g weight charge with the dimension of 150 mm x 150mm plates contained too much charge which resulted in the plate fragmenting into pieces. The thickness of the explosive was 24 mm. The equivalent pressure with this thickness was about 23 GPa in Table 6. With 600 g charge weight and 150 mm x 150 mm plate dimension with 10° inclination, the two plates produced a solid, but imperfect, bond as shown in Figure 7a. This implies that the slowdown of impact velocity will positively affect the explosive welding. With 15° inclination, however, the two plates produced a very good weld as shown in Figure 7b. The magnified images of the vertical surface are shown in Figure 8.

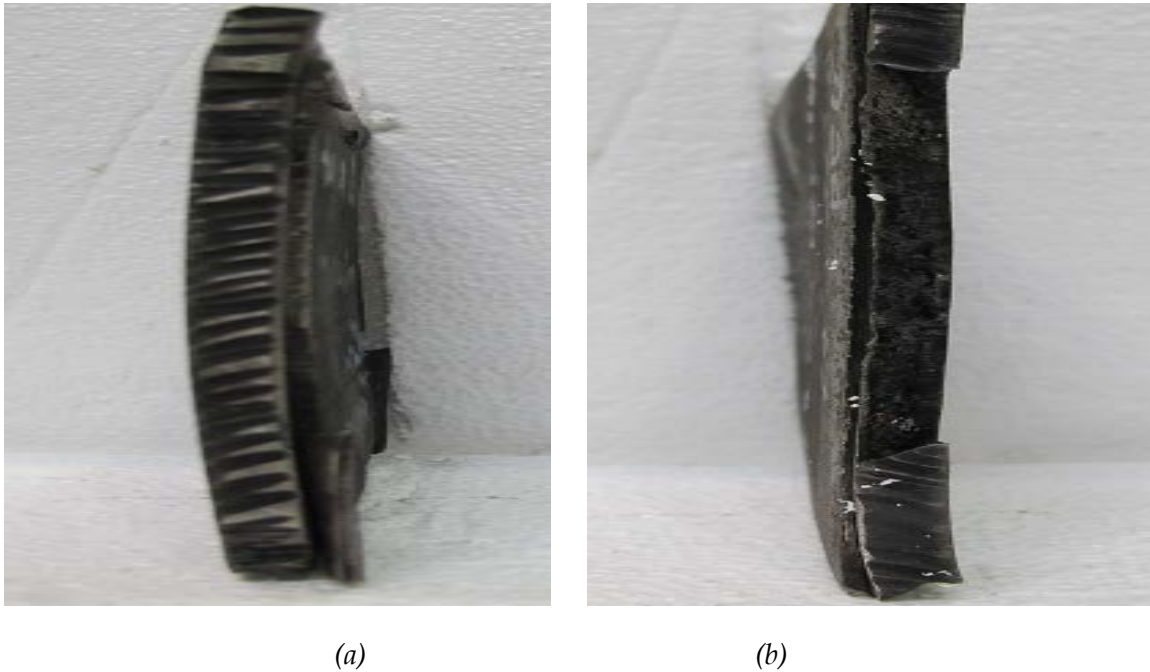


Figure 7: Explosive bonding between superaustenitic steel and TRIP steel (Test No 4)

Figure 8 shows the magnified image of the vertical surface between superaustenitic steel / TRIP steel, in which two materials possessed a good metallurgical bond, showing a wave-type morphology, also termed 'hand shake'.

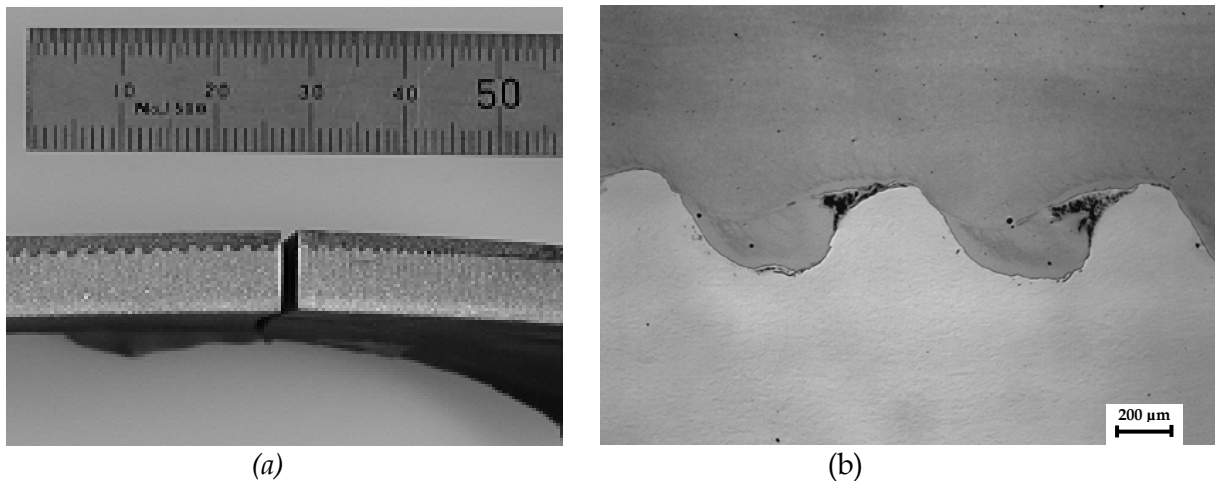


Figure 8: (a) Macrograph showing the wave-type morphology at the interface of the bonding area between a superaustenitic steel (bottom) and a TRIP steel (top). (b) Micrograph showing a higher magnification of (a)

It is clear from this work that if the angle between the flyer plate and bottom plate is controlled, the flyer plate velocity can be modified. In other words, the angle between two plates is one of the main controlling parameters to adjust the effective detonation velocity and the flyer plate velocity.

It is generally accepted that the detonation velocity should be subsonic with respect to the sonic velocity of the materials to be bonded. However, the velocity should not be too low, otherwise no

jet is created. Carpenter et al. [11] indicate that explosives with detonation velocities greater than 120% of the sonic velocity of the metal should not be used. If it is correct, the velocity of the explosive PE 4 (7900 m/s) is beyond the limit because the sonic velocity of superaustenitic steel is 5900 m/s. However, the current experimental results show that PE4 can be used as an explosive for superaustenitic steel, enabling explosive bonding with substrate steel materials provided the plates have an optimum contact angle between them.

In the final test, the sample size was increased from 150 mm x 150 mm to 300 mm x 300 mm with 15° inclination angle and 16 mm thickness of the PE4 charge (see Table 3). A 300 mm x 300 mm plate setup was used for test 5 to enable further analysis such as residual stress to be conducted.

The bottom plate was changed from soft and ductile TRIP steel to the hard and strong HARD steel. The hardness of TRIP and HARD steels in the as-received conditions were 190 HV_{200g} and 440 HV_{200g}, respectively. According to the Gurney equations, the results of No 2 and No 4 explosive bonded tests in Table 3, should be identical because the thickness of the charge used was the same, ie 16 mm. However, the superaustenitic steel to HARD steel combination was more difficult to bond than the superaustenitic steel to TRIP steel combination. It may be that hard steel is more difficult to explosively-bond. In this case, the explosive thickness confined in the charge container was calculated to be 16 mm after angle compensation. A 2.4 kg charge weight was used to maintain this thickness. It showed a good bonding but less wavy and inter-locking interface. It is reasonable to assume that harder material is less readily deformed, which will in turn produce a less wavy or inter-locked pattern at the interface. This will be discussed further in section 3.2.

Detonation vs M/C ratio

Detonation velocity against M/C relationship is shown in Figure 9. By combining Eq 5, Eq 6 and Eq 7, the detonation velocity and M/C rate can be calculated. The relationship between M/C and detonation velocity is shown in Figure 9. It shows the trend that increasing the M/C ratio results in a decrease in the detonation velocity.

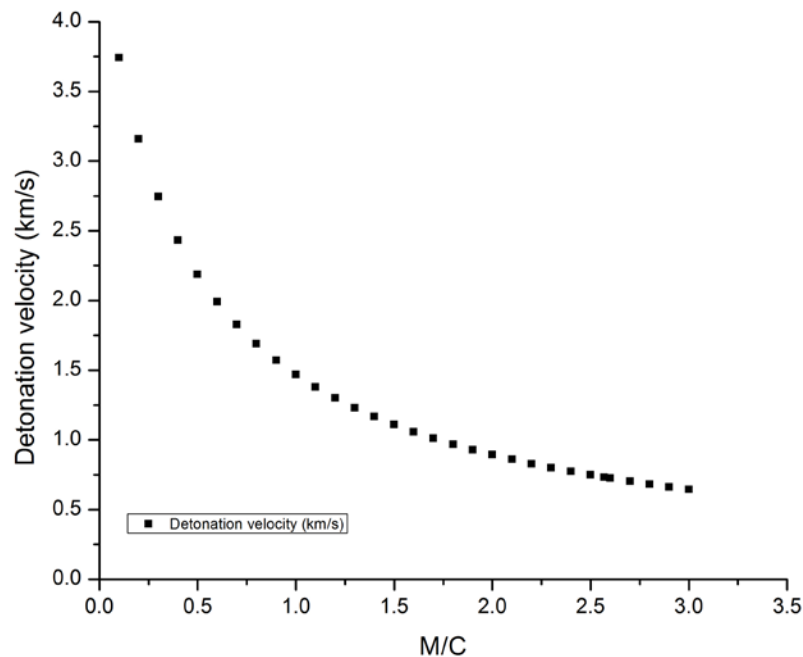


Figure 9: The relationship between detonation velocity and M/C

3.2 Investigation of microstructural and hardness variation of explosive welded joints

3.2.1 Microstructural variation

In this section, the microstructural evolution of both superaustenitic steel / TRIP steel and superaustenitic steel / HARD steel joints after explosive welding are examined and described in detail.

Superaustenitic steel / TRIP steel joint

The interface between the superaustenitic steel flyer plate and the TRIP steel bottom plate is shown in Figure 10. The TRIP steel is shown as an etched surface (dark) and the superaustenitic steel is shown as unetched (white). It is clearly evident that a wave-type morphology was produced at the interface of the materials via the explosive welding process, which resulted in a 'hand shake' pattern of joining the two material. From Figure 10, the height of the wave was observed to vary. This is because the sample examined was taken toward the end of the welded joint. The black dots in the TRIP steel surface are a result of inclusions being removed during the etching process. Further, located under some of the crests of the TRIP steel wave, were areas of lack of bonding, resulting in small void or cavity formation. These will be detailed in subsequent sections.

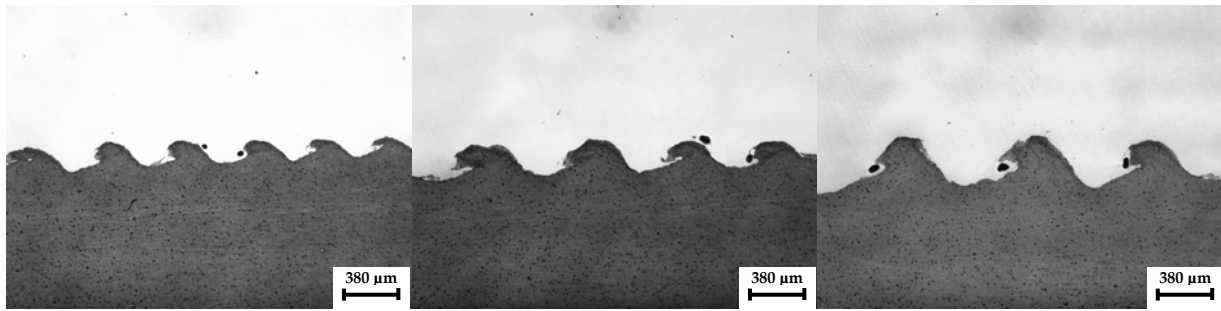


Figure 10: The wave-type morphology at the interface of the superaustenitic steel – TRIP steel joint. Variation in wave height is observed. Etched (dark) microstructure is TRIP steel and the unetched (light) microstructure is superaustenitic steel.

Figure 11 shows both TRIP steel and superaustenitic steel microstructures. The wave-morphology in both materials is easily seen and the materials appear to overlap considerably creating a good bond. The grain structures of the both steels toward and within the waves, were observed to orient in the direction of material flow, typical of the deformation direction due to the explosive welding process.

Figure 12 shows Adiabatic shear bands (ASB), which are clearly observed in the superaustenitic steel, generally occurring at the front and behind the wave itself. These ASBs are observed to penetrate significantly into the bulk plate thickness, up to approximately 1.2 mm depth. ASB are, in general, formed under conditions of high strain rate ($> 10^3/\text{s}$) with accompanying large strains and hence highly localised large deformations, which are characterised by heavily deformed grain structure and grain-refinement. As the name suggests, the deformation process occurs in essentially an adiabatic manner. The high strain rates and pressures from the explosive welding processes, result in severe plastic deformation in the materials, where a very sharp, short rise in temperature (with no time for large heat exchange into the bulk material) occurs and subsequently leads to a reduction in the flow stress of the material and therefore formation of ASB. These shear bands are generally oriented at 45° , the direction of maximum shear stress. This shear band area with the compressed depression exhibits very high strength in the order of 10 to 12 GPa as described by Syn et al [14]. It is clear at this stage that the explosive bonding creates a large strain accompanied by ASB with very high strength due to significant grain-refinement. This band is also known as 'white layers' because of their resistance to etching, as reported in previous work [14].

There was also evidence of casting structure formation at the front, on top and behind the waves of both materials, which is, maybe, due to the high localised heating that causes partial remelting of the materials during explosive bonding. It should be noted that this cast structure is usually less than $50\text{ }\mu\text{m}$ in thickness.

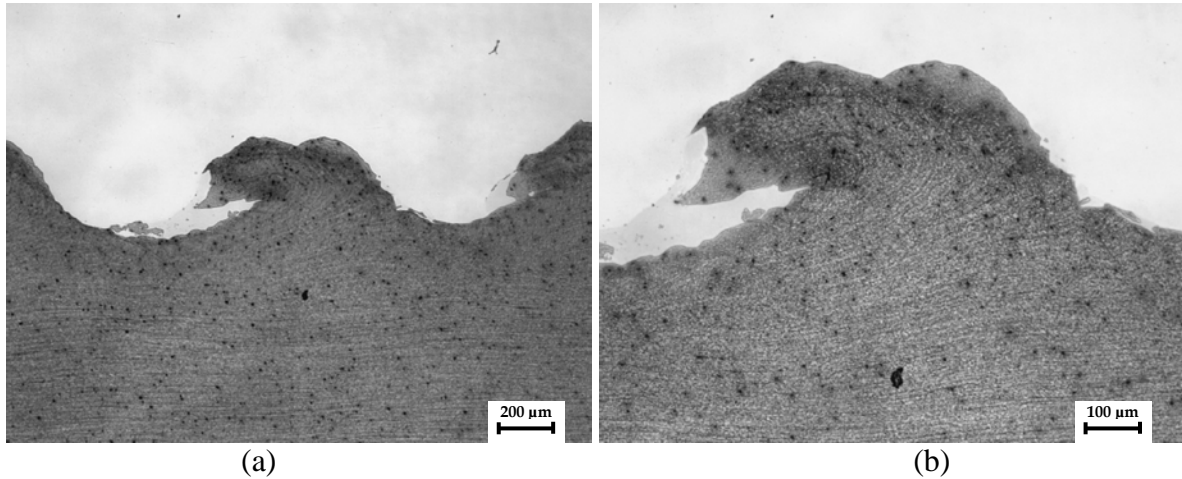


Figure 11: (a) The interface of superaustenitic steel – TRIP steel joint and (b) higher magnification depicting a single wave. Black dots are inclusions removed during etching. Etched microstructure is TRIP steel, unetched microstructure is superaustenitic steel.

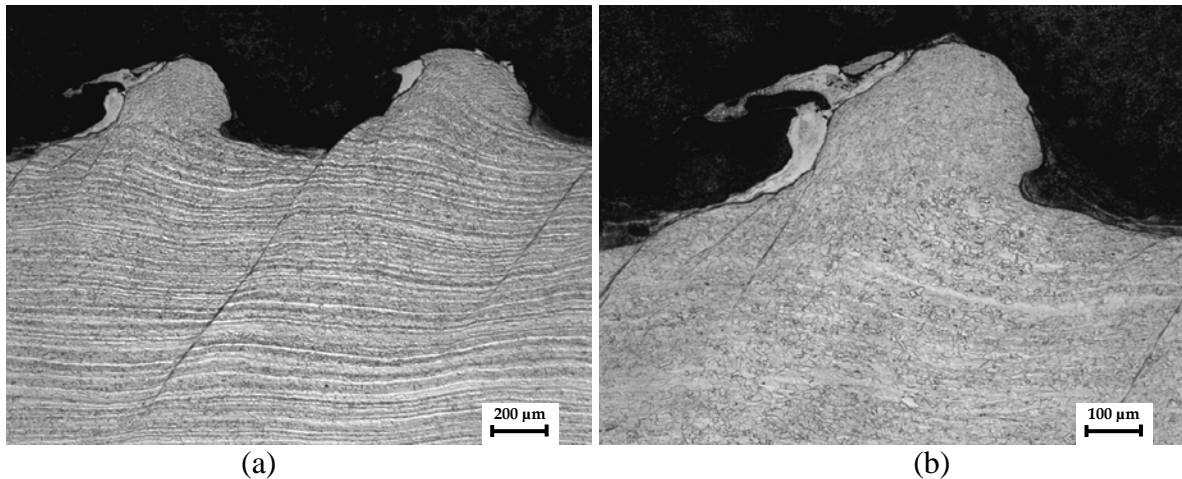


Figure 12: (a) The interface of superaustenitic steel – TRIP steel joint and (b) higher magnification depicting a single wave. Adiabatic shear bands are clearly observed. Etched microstructure is superaustenitic steel, dark microstructure is TRIP steel.

Figure 13 shows the plastic flow induced through the deformation process, with grain reorientation occurring due to jetting in both materials. ASB were observed in both materials (Figure 13b and d), however, more prevalent in the superaustenitic steel. It should be noted that the penetration depth of ASB was greater in the superaustenitic steel and could be related to mechanical properties such as the hardening exponent of both materials. That is, the amount of work hardening and subsequent strengthening of the TRIP steel at these localised regions of intense deformation, is greater than the superaustenitic steel that possesses superior ductility globally.

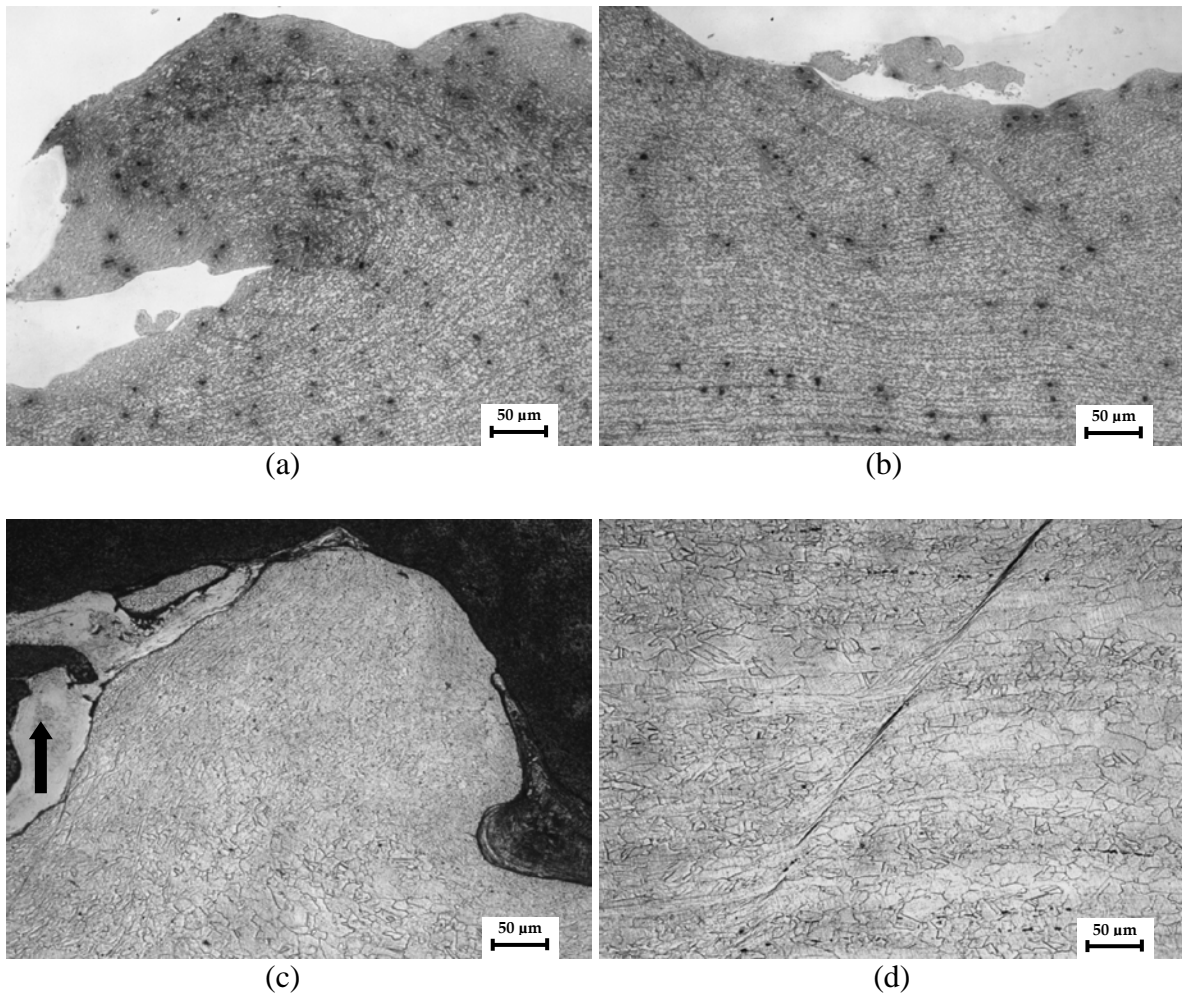


Figure 13: (a) A wave of TRIP steel with orientation of grains in the direction of materials flow (b) short-length adiabatic shear bands formation at the back of a TRIP steel wave; (c) superaustenitic steel wave showing deformation of grains as well as possible cast microstructure (marked with arrow) at the back and front of the wave; d) an adiabatic shear band within the bulk of the superaustenitic steel.

Figure 14 shows the typical grain structure in the wave regions for both materials. The ASB of the TRIP steel are observed in Figure 14a, together with the very fine grained microstructure that has been deformed within a wave. The microstructure consists of ferrite (white) and mix mode of bainite, martensite and retained austenite (dark islands in Figure 14b). The superaustenitic steel is shown in Figure 14c and d revealing deformed grains of austenite and columnar microstructure of casting structure with void defects present at the front of a superaustenitic wave (Figure 14e). These areas possess the microstructure of the superaustenitic steel.

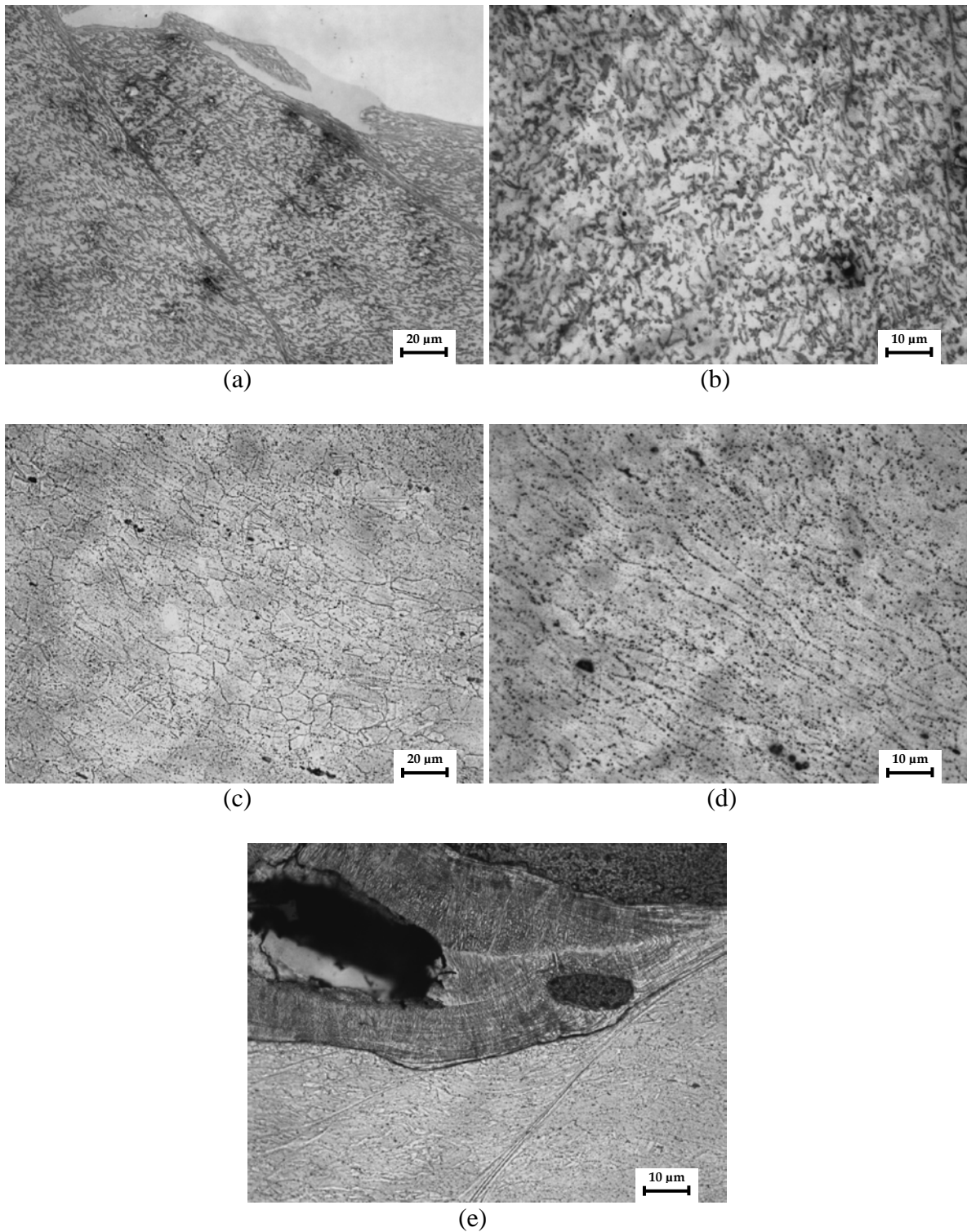


Figure 14: (a) Adiabatic shear bands at the back of a TRIP steel wave; (b) deformation microstructure of TRIP steel within a TRIP steel wave; (c) and (d) deformed microstructure within a super austenitic wave; (e) casting structure showing cellular microstructure and columnar grains as well as voids.

Superaustenitic steel –HARD steel joint

The interface between the superaustenitic steel flyer plate and the HARD steel bottom plate are shown in Figure 15. The HARD steel is shown through an etched surface (dark) and the superaustenitic steel is shown as unetched (white). As was mentioned for the TRIP steel joint, it is clearly seen that a wave-type morphology was produced at the interface of both materials which resulted in a 'hand shake' pattern of bonding between the two materials. The height of waves were very consistent in this sample. There were regions at the front of the HARD steel wave that showed voids coinciding with voids within casting structures, as had occurred in the TRIP steel joint. This will be examined in further sections.

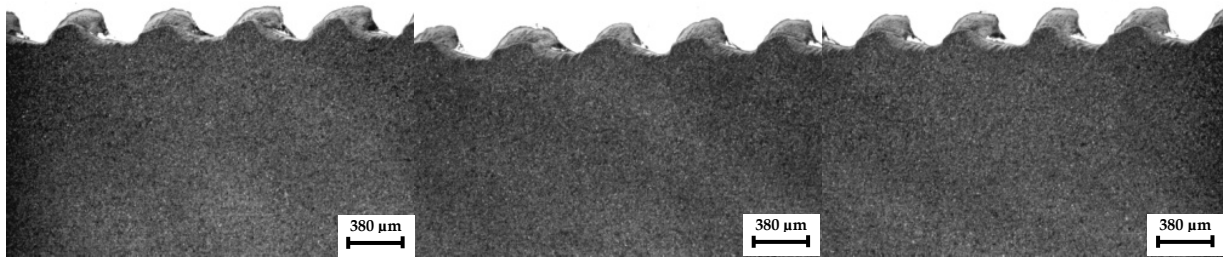


Figure 15: The wave-type morphology at the interface of the superaustenitic steel –HARD steel joint. Etched (dark) microstructure is HARD steel and the unetched (light) microstructure is superaustenitic steel.

ASB are evident in HARD steel; in Figure 16a and Figure 16b for each wave. ASB are located at the front and back of each wave and also within each wave (appears lighter in etching). It should be noted that each wave possessed a large ASB within the centre of the wave, where the wave was folded due to the joining processes. It appears that due to the hard and strong martensitic structure, with limited ductility, shear banding is the predominant deformation mode. ASB were found to be between 50 to 100 μm in length at the front and back of the waves. In great contrast, the superaustenitic steel revealed much less ASB than in the superaustenitic steel / TRIP steel joint. This may be due to the limited global deformation allowed by the harder, stronger HARD steel. Moreover, the ASB were located at the back of each wave, with the first band possessing $\sim 200 \mu\text{m}$ depth, followed by 3 to 5 bands of lesser depth of penetration.

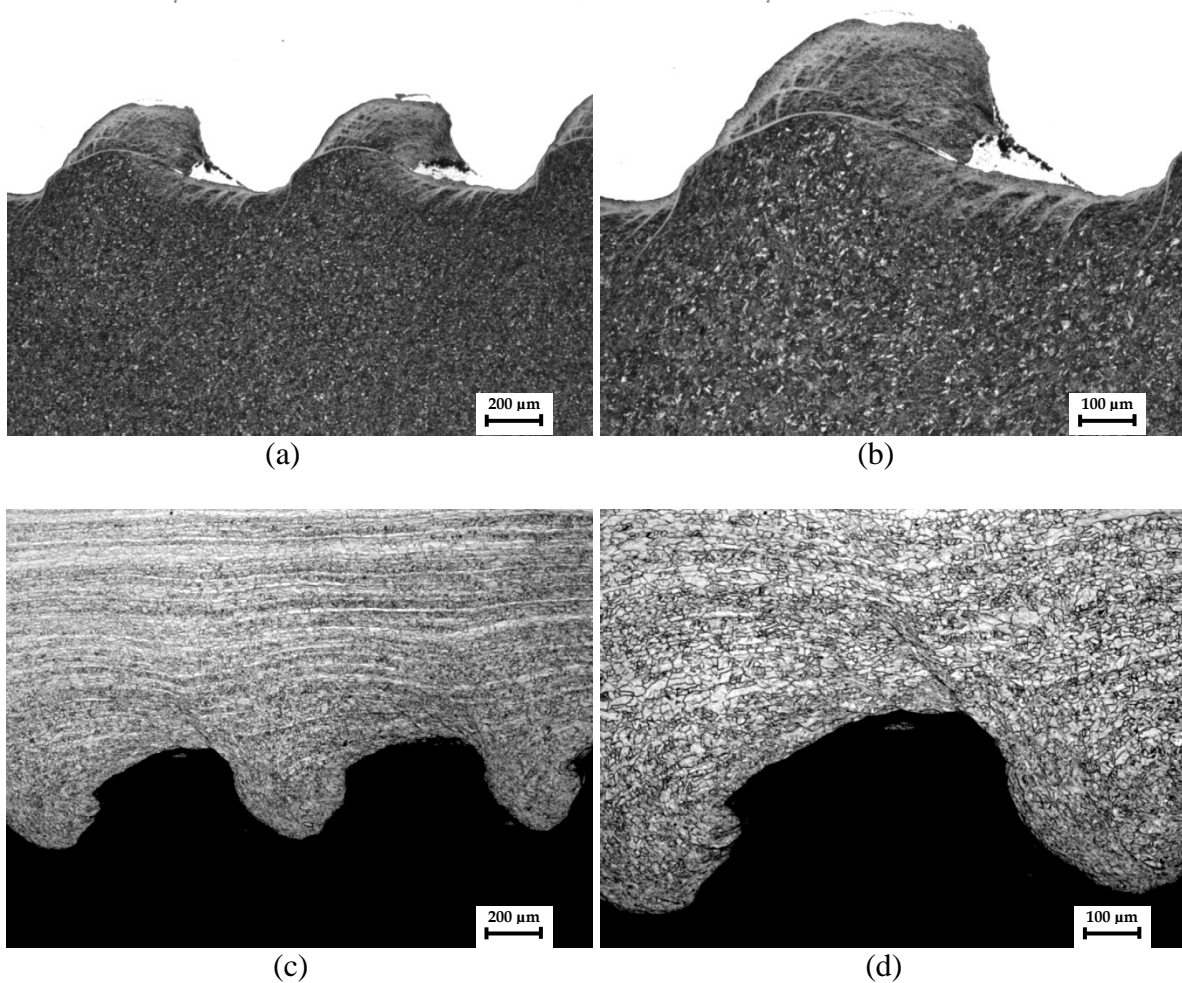


Figure 16: (a) and (b) Wave-type morphology and adiabatic shear bands in martensitic steel (a) (b) scale bar 100 μm ; (c) and (d) Segregation banding and wave morphology with few adiabatic shear bands in austenitic steel (martensite etched dark).

Figure 17 shows higher magnification wave-like morphology of each material. Plastic flow is readily seen, resulting in refining of grain structure through shear. Typical martensitic microstructure that has been undeformed, is observed in the HARD steel at small depths below interface, indicating that only subsurface deformation is present within the first 0.5 to 1.0 mm of plate thickness. However, deformation is observed in the supraustenitic steel at much greater depths. At the front and back of each wave, some casting structure is observed with voids present. As in the supraustenitic - TRIP steel interface, these areas of solidified melt, suggesting high temperatures reached during welding, possessed austenitic microstructure.

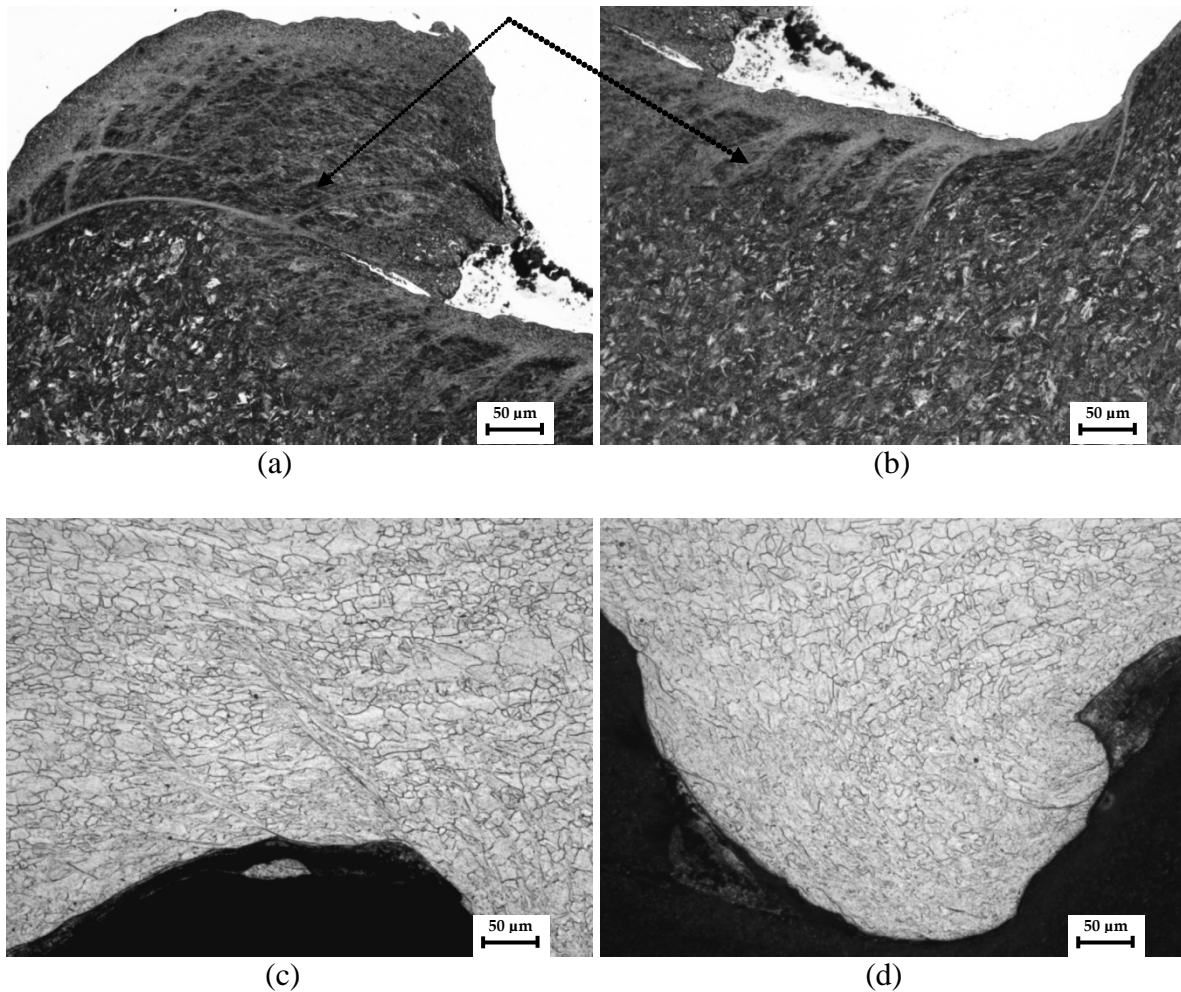


Figure 17: (a) and (b) Wave-type morphology, adiabatic shear bands and deformation grain in martensitic steel. Dark area at front of martensitic wave shows voids within the cast structure (arrows); (c) and (d) austenitic steel revealing adiabatic shear band and the deformation and re-orientation of grains due to plastic flow.

The metallurgical complexities of this joint system become readily apparent in Figure 18. Figure 18a shows ASB formation within a HARD steel wave and also grain morphology that appears to take the form of recrystallised grains. These grains are adjacent to the casting structure that has reached very high temperatures to induce melting, which result in subsequent localised heat-treatment and grain growth of deformed grain structure of the tempered martensitic structure. Further, this grain structure is also observed in Figure 18c at the front of the wave and above ASB. Again, this grain structure is located under the cast structure. Figure 18 b reveals the front of the HARD steel wave, with large amounts of voids within cast structure.

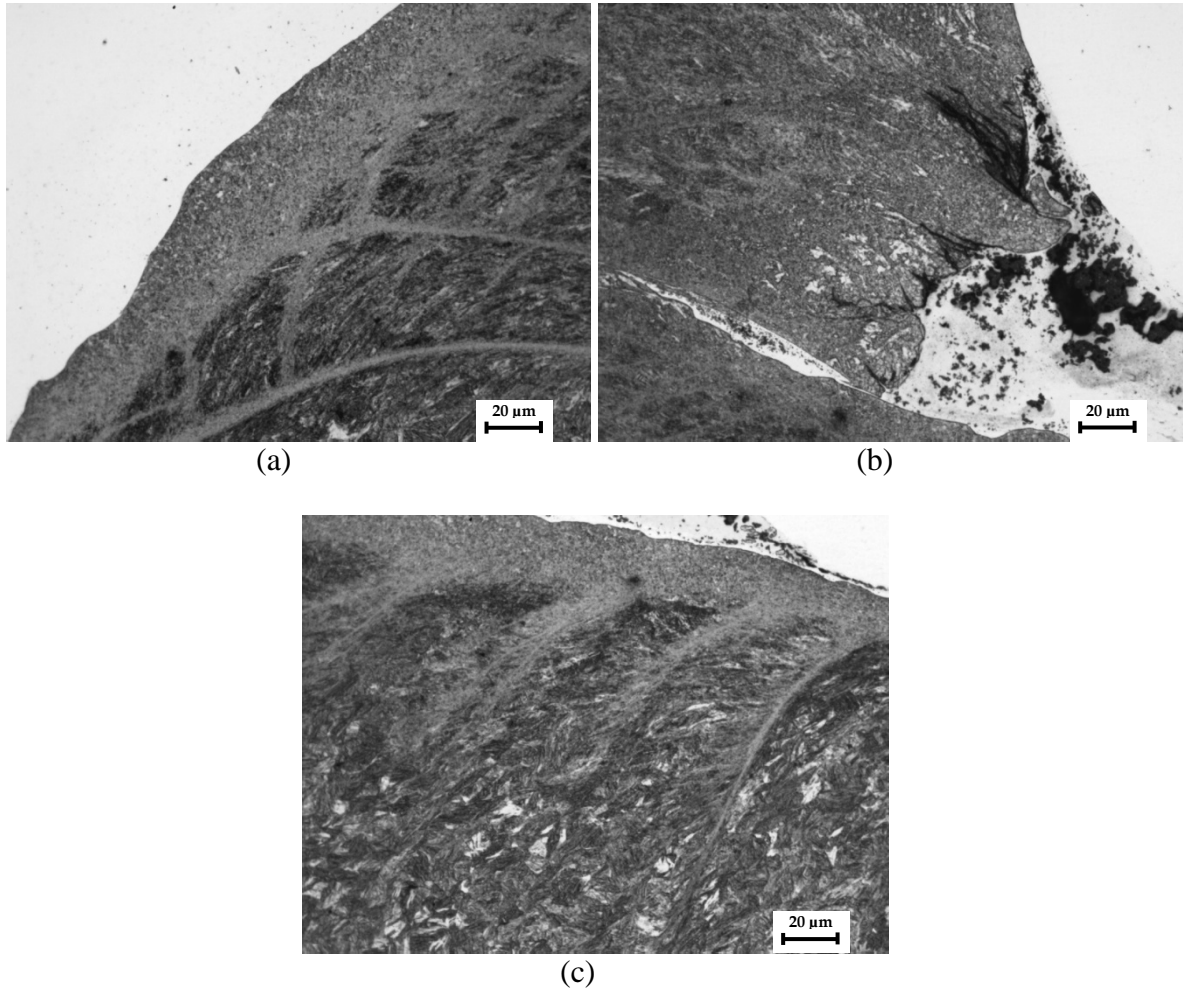


Figure 18: (a) to (c) Higher magnification of martensitic wave and adiabatic shear band formation

Figure 19 depicts the superaustenitic steel, with the grain deformation in the multiple directions of plastic flow in the material (19a and b). Figure 19c shows ASB formation in the superaustenitic steel.

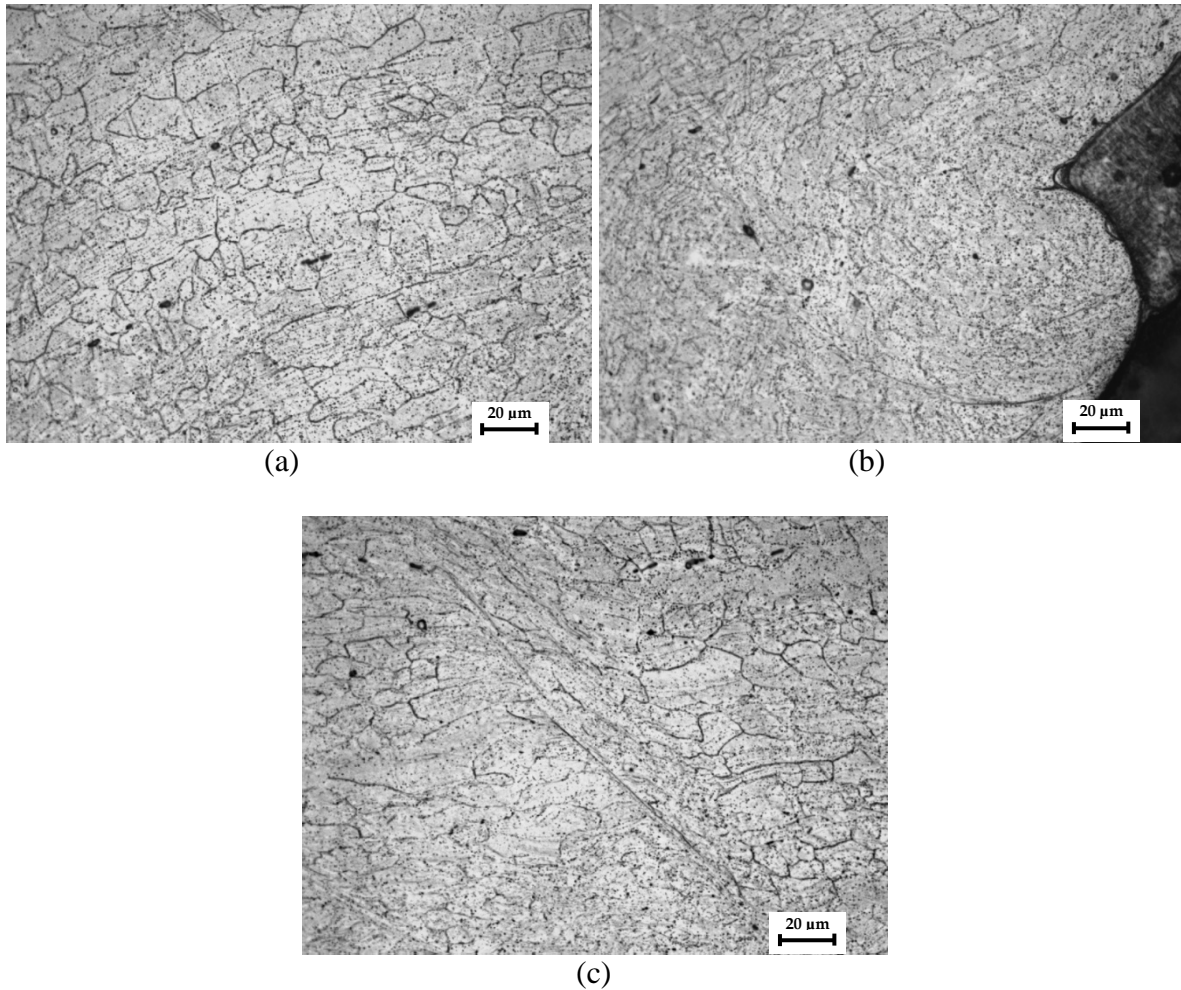


Figure 19: (a) and (b) The deformed grains within a wave of superaustenitic steel; (c) adiabatic shear band formation within superaustenitic steel

3.2.2 Joint Hardness Variation

The through-thickness microhardness measurements of as-received materials prior to explosive welding are shown in Table 8, as an average measurement across the through-thickness. There was little variation in hardness observed through-thickness. As can be seen from Table 8, the superaustenitic steel flyer plate was lower in hardness than either of the bottom plate materials in these experiments.

Table 8: Hardness values of as-received superaustenitic steel, TRIP steel and HARD steel, prior to explosive bonding

Material	Hardness (HV _{200g})
superaustenitic steel	215
TRIP steel	250
HARD steel	440

The hardness evolution measured in the through-thickness direction of the superaustenitic steel – TRIP steel and superaustenitic steel – HARD steel joints after explosive welding are shown in Figures 20 and Figure 22, respectively. The hardness evolution of each material, in each combination, will be described in this section.

Superaustenitic steel – TRIP steel joint

The hardness of the superaustenitic steel can be separated into 4 hardness zones, as follows:

1. From the interface with TRIP steel to a thickness of approximately 1.5 mm below, hardness values were between 420V to a peak hardness of 480 HV
2. From approximately 1.5 mm to 3.3 mm below interface, the hardness range was quite similar, that is between 412 and 420 HV
3. From approximately 3.8 to 6.8 mm below interface, the hardness range was 370 HV to 400 HV
4. The final point, taken closest to the impact of the blast showed some working hardening with a value of 410 HV.

At zone 1, significant localised deformation was observed and this can account for the increase in hardness, as this zone corresponded to areas of severe localised plastic deformation, reduced grain-size and adiabatic shear band formation (Figure 21a). From zone 2 to 3, hardness appeared to reduce in steps and this reduction is most likely due to lesser deformation occurring through-thickness. Finally, in zone 4, the increase in hardness observed may be a result of the global deformation of this plate from the blast itself, inducing work-hardening toward the surface of the plate exposed to the blast. It is noteworthy that even zone 4 hardnesses (370 – 400 HV) were considerably higher than the original material (215 HV)

In contrast with the superaustenitic steel, the TRIP steel showed an exponential reduction in hardness from a peak of 485 HV to approximately 300 HV, from the interface to 0.6 mm below. The first three hardness indents within the highly deformed microstructure are shown in Figure 21b. In another sense, the work-hardening occurred in a stable manner. After this point, the hardness was found to be steady at 300 HV throughout the remaining plate thickness. This signifies only localised deformation occurring in the first quarter of plate thickness, due to the nature of

transformation-induced plasticity or work-hardening in this steel, occurring from the transformation of residual austenite to martensite, hence enhancing strength in this zone. This zone would typically have larger amounts of martensite phase constituent and together with the severe plastic deformation refining grain size, the hardness is therefore increased.

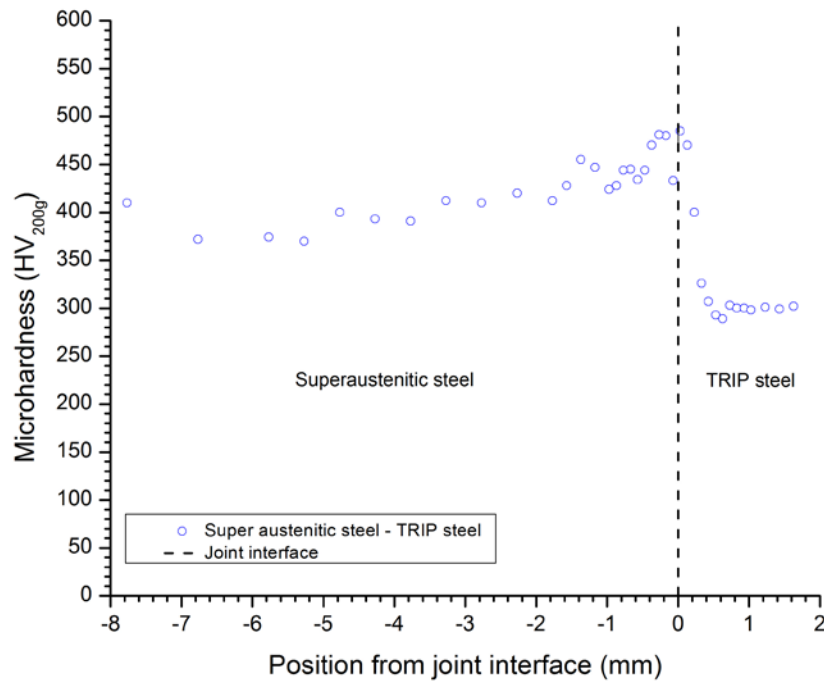


Figure 20: Microhardness variation in the through-thickness direction of the superaustenitic steel – TRIP steel explosive welded joint

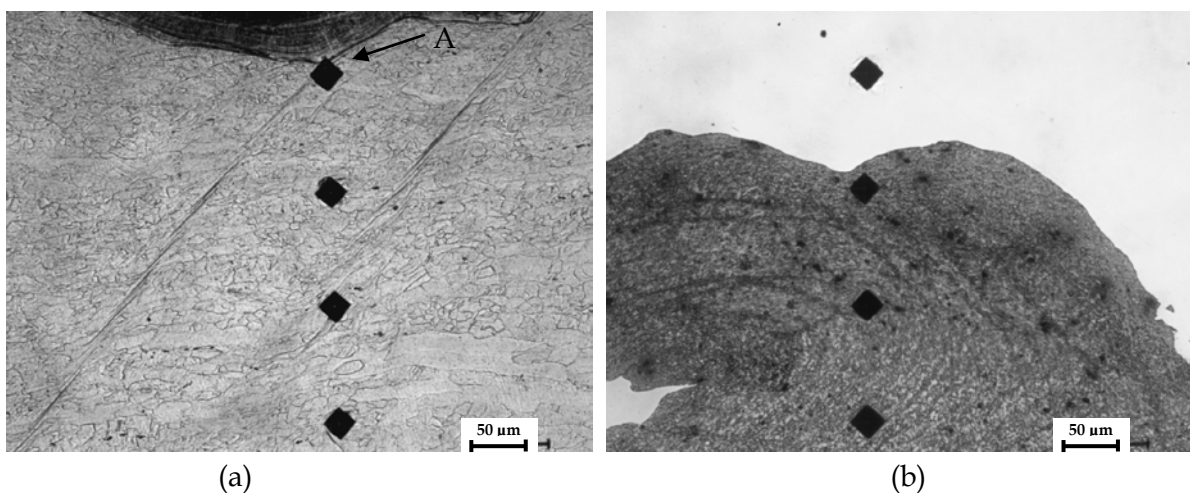


Figure 20: Microhardness indentation measurements in (a) superaustenitic steel and (b) TRIP steel. Mark 'A' shows the position of the maximum hardness.

Superaustenitic steel –HARD steel joint

In similar behaviour with the TRIP steel combination, the superaustenitic steel displayed distinct zones in combination with HARD steel, described as follows:

1. From the interface with HARD steel to approximately 1.5 mm below, the hardness ranged from 416 HV to a peak of 505 HV. This is due to the severe plastic deformation occurring toward the interface, grain-refinement and the formation of adiabatic shear bands, as shown previously in Figure 23
2. From approximately 2 mm to 3.5 mm below the interface, hardness was observed to step down and reduced from 400 to 350 HV. This was due to the lesser work-hardening occurring in this thickness region
3. After 3.5 mm below the interface, the hardness was found to be steady at 350HV for the remaining plate thickness. Further, it should be noted that no work hardening was observed at the surface exposed to the blast, as found for the superaustenitic steel – TRIP steel joint (to be published separately).

The HARD steel was seen to behave differently, with a peak hardness of 585 HV reached at the interface, followed by significant and sudden reduction to ~500 HV after 0.65 mm below interface (Figure 21) after which hardness was found to be steady around ~500 HV for the remaining plate thickness. The peak hardness is a result of the localised plastic deformation and ASB formation as observed in Figure 23. However, the sharp reduction in hardness to the base level of 500 HV is a result of the smaller depth of deformation (see Figure 23, the final hardness indentation is within undeformed martensitic structure) and the high strength and hardness, as well as limited ductility of the martensitic structure, with this steel typically displaying no more than 10-15% elongation.

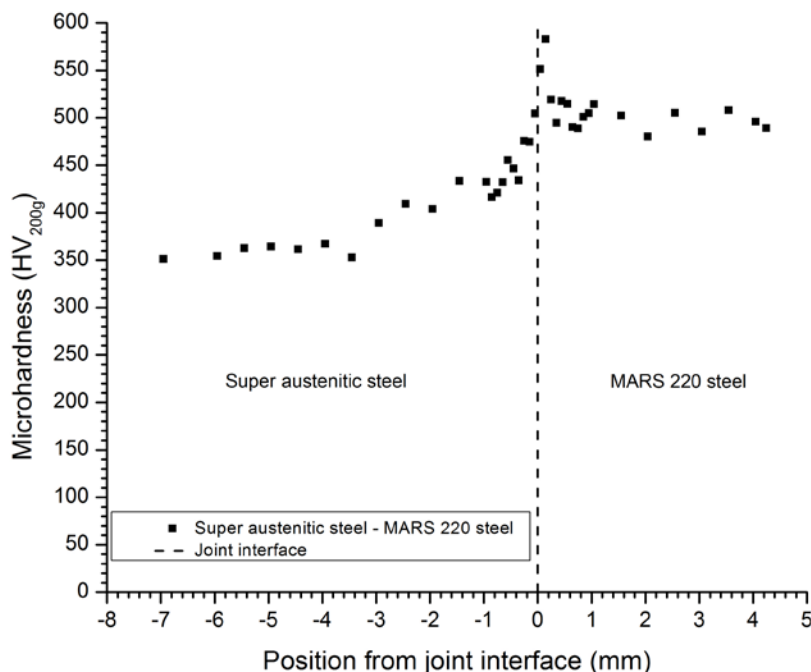


Figure 21: Microhardness variation in the through-thickness direction of the superaustenitic steel –HARD steel explosive bonded joint

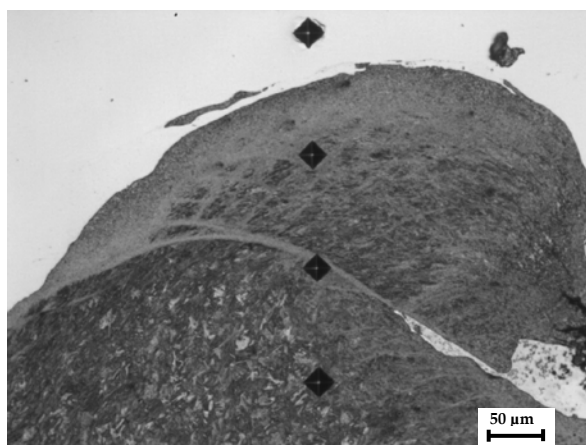


Figure 22: Microhardness indentation measurements in the HARD steel (etched surface)

Comparison of joints

Figure 24 shows a hardness profile comparison of the two explosive bonded joints. The behaviour of the superaustenitic steel flyer plate is similar from the interface to approximately 3.0 mm below the interface for both joint combinations. After this point, the behaviour does slightly change, with the TRIP steel combination reducing in hardness over a greater plate through-thickness. This may in part be due to the higher ductility of the TRIP steel, allowing greater global deformation of the superaustenitic plate during explosive welding, in comparison with the harder, stronger and less ductile HARD steel. It may be pertinent at a later stage, to consider numerical modelling analyses of these joint combinations, to determine if this is the case, or this is simply due to material batch variation or small differences in experimental parameters during the joining process.

Significant differences in the level of ductility and hardness of both bottom plates of TRIP and HARD steels was expected due to processing, chemistry and phase constituents present in each steel. However, the one similarity is that both these steels, regardless of thickness, or metallurgical or mechanical properties, reduced from peak hardness to a steady-state hardness level at approximately 0.6 mm from the interface with the superaustenitic steel flyer plate.

It is noteworthy that all three materials (superaustenitic, HARD and TRIP) showed hardening in the base metal as a consequence of the blasting process. This suggests that all would show improvement in blast and ballistic performance as a consequence of blast-related work hardening.

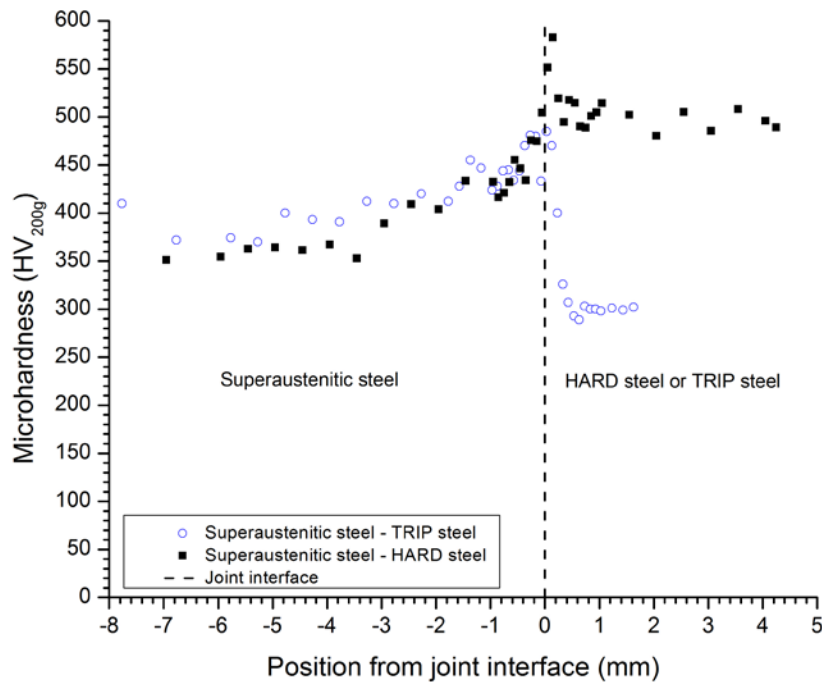


Figure 23: A comparison in the microhardness variation in the through-thickness direction both the superaustenitic steel – TRIP steel and superaustenitic steel –HARD steel explosive welded joints.

4. Conclusions

Explosive bonding was conducted on two candidate material combinations, utilising different plate configurations, that possessed an elevated angle between flyer and bottom plates, supersonic velocity explosive and plate materials of different processing, chemistry and mechanical properties. A number of key findings have been determined through this study and are described as follows:

The Gurney equations may be used as a guideline to control M/C ratio, charge thickness, and contact velocity (such as an upper bound and lower bound window) for producing explosive bonding of armour material, utilising a combination of materials properties including high strength and hardness, as well as high toughness and ductility, depending on the plate material configurations used.

From these results, it appears that explosive material possessing supersonic velocity such as PE4, may be used with modified Gurney equations, by controlling elevation angle between the flyer and bottom plates. The bottom plate hardness should also be taken into consideration when applying the Gurney equation to the explosive bonding process.

Both superaustenitic steel – TRIP steel and superaustenitic steel – HARD steel joint combinations produced a fair and good explosively welded joints with wave-type morphology at the interface

between flyer and bottom plates, hence ensuring a good metallurgical bond. The superaustenitic-TRIP steel produced a better joint than the superaustenitic –HARD steel combination.

The microstructural evolution of superaustenitic steel, TRIP steel and HARD steel plates, when subjected to the explosive bonding process, produce complex metallurgical phenomena at the joint interface. These include areas of intense localised deformation inducing plastic deformation, work-hardening and subsequent materials flow, that orient grain structure; areas of possible solidified melt casting structure, voids; refinement of grain size, recrystallisation; and adiabatic shear band formation. The extent to which these phenomena occur, is indeed related to the type of material and their metallurgical properties, but also importantly, it must be noted that it is affected by the joint combination.

The hardness increase measured at the through-thickness of each joint yielded interesting information on the amount of deformation-induced effects and work-hardening as a result of the bonding process. This correlated to the metallurgical phenomena that were present in the microstructure, particularly, with respect to strain-hardening and consequent increase in both hardness and strength. Interesting, the hardness increase resulting from work-hardening observed in the bottom plates, reduced to a steady-state level after approximately 0.6 mm depth; and the flyer plate hardness was relatively similar for both joint configurations.

5. Acknowledgements

The authors gratefully acknowledge for John Williams and Trevor Delaney for his assistance during the testing.

6. References

- [1] F. Findik, 'Recent developments in explosive welding', *Mater Design*, vol 32, 2011, p1081-1093.
- [2] M. Acarer, B. Gulenc, F. Findik, 'Investigation of explosive welding parameters and their effects on microhardness and shear strength', *Mater Design*, vol 24(8), 2003, p659-664.
- [3] A. Ghanadzadeh, A. Darviseh, 'Shock loading effect on the corrosion properties of low-carbon steel', *Mater Chem Phys*, vol 82, 2003, p78-83.
- [4] F. Grignon, D. Benson, K.S. Vecchio, M.A. Meyers, 'Explosive welding of Aluminium to Aluminum analysis, computations and experiments', *Int J Impact Eng*, vol 30, 2004, p1333-1351.
- [5] J.H. Han, J.P. Ahn, M.C. Shin, 'Effect of interlayer thickness on shear deformation behaviour of AA5083 aluminium alloy/SS41 steel plates manufactured by explosive welding', *J Mater Sci*, vol 38, 2003, p13-18.
- [6] V. Balasubrahmanian, M. Rathinasabapathi, K. Raghukandan, 'Modelling of process parameters in explosive cladding of mild steel and aluminium', *Mater Process Technol*, vol 63, 1997, p83-88.
- [7] M. Acarer, B. Demir, 'An investigation of mechanical and metallurgical properties of explosive welded aluminium–dual phase steel', *Mater Lett*, vol 62(25), 2008, p4158-4160.
- [8] A. Durgutlu, B. Gulenc, F. Findik, 'Examination of copper/stainless steel joints formed by explosive welding', *Mater Des*, vol 26 (6), 2005, p497-507.
- [9] R. Gurney, 'The initial velocities of fragments from bombs, shells, and grenades', Report No 405, Ballistic Research lab, Aberdeen, MD, Sep, 1943, AII-36218.
- [10] A. Marc. Meyers, Chapter 9-2, 'Dynamic Behaviour of materials', 1994, John Willey & Sons, Inc.

- [11] S.H. Carpenter and R.H. Wittman, 'Explosion welding', *Annu Rev Mater Sci*, 1975. vol 5, p177-199.
- [12] S. Carpenter, R.H. Wittman, R.J. Carlson, '*Relationships of explosive welding parameters to material properties and geometry factors In: Proc first int conf of the centre for high energy forming*', University of Denver; June 1967. p. 124.
- [13] A.M. Meyers, '*Dynamic Behavior of Materials*', John Wiley & sons, Inc., 1994, p244-270, p609.
- [14] C.K. Syn, D.R. Lesuer, O.D. Sherby, '*Microstructure in adiabatic shear bands in a pearlitic ultrahigh carbon steel*', *Mater Sci Tech*, Vol 21(3), 2005, p317-324.
- [15] R.H. Wittman, Proc. 2nd intl. Symposium on the use of Explosive Energy manufacturing Metallic materials, Marian Sic laxne, Czechoslovakia, 1973.
- [16] A.A. Deribas, V.F. Nesterenko, T.S. Teslenko, '*Universal dependence of the metal hardening parameters on the intensity of shock action*', *Combustion, Explosion, and Shock Waves*, vol 18, 1982, p670-675.
- [17] P.W. Cooper, '*Explosives Engineering*', Wiley-VCH, Inc, 1996, ISBN: 0-471-18636-8, p179-201.

Appendix A

Gurney Equation

The governing factor of the Gurney equation [9] is the fragment velocities from blasting related to the ratio between the mass of the fragments (M) and the mass of the explosive (C), under the assumption that the chemical energy of the explosive was transformed into kinetic energy of the explosive products and metal fragments. Gurney arrived at expressions relating the velocity of fragments to the ratio M/C .

Cylindrical geometry

The total kinetic energy of the fragments is given by

$$KE = \frac{1}{2} \sum m_i V_o^2 + \int V^2 dm_g \quad (A1)$$

where m_i = the mass of the i^{th} fragment, dm_g = element mass in the gases, V = fragment terminal velocity and V_o = initial fragment velocity.

$$dm_g = \rho dV = 2\pi r \rho dr \quad (A2)$$

where ρ = explosive density and r = radius of element gas in cylindrical shape.

Under the assumption that all the fragments have the same velocity, eq. (2) can be inserted into eq. (1).

$$KE = \frac{1}{2} V_o^2 + \frac{1}{2} \int_0^a V_o^2 \frac{r^2}{a^2} 2\pi r \rho dr \quad (A3)$$

where a is the radius of cylindrical shell filled with explosive and

$$\frac{C}{\pi a^2} = \rho \quad (A4)$$

and

$$KE = \frac{1}{2} M_i V_o^2 + \frac{1}{4} C V_o^2 \quad (A5)$$

From these equations, the terminal velocity can be derived as a function of the ratio M/C ,

$$V_o = \sqrt{2E} \left(\frac{M}{C} + \frac{1}{2} \right)^{-\frac{1}{2}} \quad (A6)$$

where E is the Gurney Energy.

Critical impact pressure

Formation of a jet is considered a prerequisite for explosive bonding. Therefore, the pressure should be sufficient, in order to allow jetting to occur at the collision point of the flyer and bottom plate materials. Wittman [14] and Deribas [15] found that a pressure equal to five times the strength of the material was necessary for jet formation (see Table 2).

It is reasonable to study Bernoulli's equation as shown in [12] to in order to determine the experimental parameters in which jetting will occur. From Bernoulli's equation:

$$p = \frac{1}{2} \rho \cdot U_p^2 \quad (A7)$$

Making U_p (particle velocity) = V_p (the plate velocity) and the pressure equal to $k \sigma_y$ ($k \sim 5$)

$$V_p = \left(\frac{k \sigma_y}{\rho} \right)^{1/2} \quad (A8)$$

This becomes the lower boundary with minimum velocity. The upper boundary is expressed as (the derivation is omitted):

$$V_p = k_2 \frac{(T_{mp} C_0 k C_p)^{1/2}}{V_C t^{1/4}} \quad (A9)$$

Where k_2 is a constant, C_0 = the bulk sound velocity, t = the flyer plate thickness, T_{mp} = melting point, k = the thermal conductivity, and C_p = the heat capacity .

Below the lower bound and above the upper bound, there is no jetting and no wave. The pressure can be measured by Rankine-Hugoniot [13, 17] equation as follows:

$$P = \rho C_0 V / 2 \quad (A10)$$

Where ρ = density of the top plate, C_0 = sound velocity of the plate, V = impact velocity (refer Table 4).

Page classification: UNCLASSIFIED

DEFENCE SCIENCE AND TECHNOLOGY ORGANISATION DOCUMENT CONTROL DATA					
				1. PRIVACY MARKING/CAVEAT (OF DOCUMENT)	
2. TITLE Modification of the Gurney Equation for Explosive Bonding by Slanted Elevation Angle			3. SECURITY CLASSIFICATION (FOR UNCLASSIFIED REPORTS THAT ARE LIMITED RELEASE USE (L) NEXT TO DOCUMENT CLASSIFICATION) Document (U) Title (U) Abstract (U)		
4. AUTHOR(S) C. Choi, M. Callaghan, P. van der Schaaf, H. Li, and B. Dixon			5. CORPORATE AUTHOR DSTO Defence Science and Technology Organisation 506 Lorimer St Fishermans Bend Victoria 3207 Australia		
6a. DSTO NUMBER DSTO-TR-2960		6b. AR NUMBER AR-015-932		6c. TYPE OF REPORT Technical Report	
7. DOCUMENT DATE April 2014					
8. FILE NUMBER		9. TASK NUMBER ?????????		10. TASK SPONSOR ?????????	
				11. NO. OF PAGES 32	
				12. NO. OF REFERENCES 17	
13. DSTO Publications Repository http://dspace.dsto.defence.gov.au/dspace/				14. RELEASE AUTHORITY Chief Land Division	
15. SECONDARY RELEASE STATEMENT OF THIS DOCUMENT <p style="text-align: center;"><i>Approved for Public Release</i></p> <p>OVERSEAS ENQUIRIES OUTSIDE STATED LIMITATIONS SHOULD BE REFERRED THROUGH DOCUMENT EXCHANGE, PO BOX 1500, EDINBURGH, SA 5111</p>					
16. DELIBERATE ANNOUNCEMENT No Limitations					
17. CITATION IN OTHER DOCUMENTS Yes					
18. DSTO RESEARCH LIBRARY THESAURUS Bonding, Welding, Explosive bonding					
19. ABSTRACT Using a modified Gurney equation, explosive bonding has been achieved with an angle of elevation between two plates and utilising an explosive charge with supersonic detonation velocity. Two joint combinations were produced with superaustenitic steel as the flyer plate and either <u>T</u> ransformation <u>I</u> nduced <u>P</u> lasticity (TRIP) steel or HARD steel as alternatives for use as bottom plates. Good metallurgical bonds were created for each joint combination, with the formation of wave-type microstructural morphology at the joint interface. As a result of localised severe plastic deformation and subsequent work-hardening within the steels the microstructures at the joint interface revealed complex metallurgical phenomena, which correlated strongly with hardness evolution.					

Page classification: UNCLASSIFIED